ATOMIC AND MOLECULAR COLLISIONS

Robert E. Johnson *University of Virginia*

GLOSSARY

Born approximation: First-order estimate of the collision cross sections.

Born–Oppenheimer approximation: Separation of the electron and nuclear motion. The latter is often treated classically.

Charge exchange: Process of transferring an electron from one of the colliding particles to the other; usually from a neutral to an ion.

Cross section: Probability of an interaction between two colliding particles expressed as an area.

Differential cross sections: Cross sections that are functions of one of the collision results (e.g., angle scattered; energy transfer). Summing over all possible results gives the cross section.

Elastic collision: Collision involving a deflection of the colliding particles but no change in their internal state.

Impact parameter: Defines the closeness of a collision as that component of the distance between the two colliding particles that is perpendicular to their relative velocity.

Inelastic collision: Collision resulting in a change in the internal states of the colliding particles.

Interaction potentials: Net change in potential energy of the two colliding particles. A potential exists for each set of initial states of the particles.

Mean free path: Average distance between encounters for a particle traversing a material.

Semiclassical method: Calculation of wave-mechanical effects using classical quantities.

Stopping cross section: Product of cross section and the energy loss in an inelastic process, summed over all such processes.

Stopping power: Stopping cross section times the material number density. Gives the energy loss per unit path length for a particle traversing a material.

The field of atomic and molecular collisions involves the study of the effects produced by the motion of atomic and molecular particles when they approach each other. The effects produced are generally described in terms of the amount of energy transferred between the colliding particles. This may be simply an elastic energy transfer corresponding to a deflection or an inelastic energy transfer producing changes in the internal states of the particles. The study of these changes is used to determine the details of the forces of interaction between atomic and molecular particles. In addition, knowledge of these effects is used to describe phenomena in which collisions play an important role, such as the behavior of gases and plasmas and the modification of solids by ion bombardment.

I. Introduction

A. OVERVIEW

The need to understand the behavior of colliding atoms and molecules is self-evident as we live in a world constructed from atomic building blocks. It is a dynamic construction of moving particles governed by a few fundamental forces. The interaction between moving atoms or molecules is thought of as a collision, and the effects produced by these collisions are a primary con-

ENCYCLOPEDIA OF PHYSICAL SCIENCE
AND TECHNOLOGY, VOL. 2

cern of this chapter. In addition, ever since Rutherford's discovery of the nucleus, collisions between atoms have provided a means of determining atomic structure and the forces of interaction. Therefore the field of atomic and molecular collisions has been sustained both by investigations into the nature of the interactions and by application of the results to help understand our atomic and molecular environment. [*See* PARTICLE ACCELERATORS.]

Collision events are correctly described via quantum mechanics (wave mechanics), but it has become customary when discussing such events to employ classical notions. In some cases this simplifies the understanding of the physics, in which case wave-mechanical effects, such as interference and diffraction, can then be incorporated as corrections. Such an approach is referred to as a semiclassical method, of which there are a variety. Basically they all have the same justification: that is, they are employed when the quantum-mechanical wavelength associated with the collision is small compared to the dimensions of the system. This is the same basis for using geometric optics to approximate the passage of light through a medium. When discussing collisions, the incident "radiation" is a beam of particles and the medium is the field of a "target" atom or molecule. The wavelength is then given by $\lambda = h/p$ where h is Planck's constant and p is the momentum of the particles. Comparing λ to an atomic radius (e.g., a_0, the Bohr radius), we establish a rough criteria for the usefulness of semiclassical methods: collision energies much greater than a Rydberg (27.2 eV) for incident electrons and much greater than hundredths of an electron-volt for incident ions, atoms, or molecules. For the heavy particles, therefore, this criterion is satisfied for most energies of interest. Care must be taken, however, in making such a statement. Diffraction regions (i.e., scattering at small angles) are *always* dominated by wave-mechanical effects, as are regions in which transitions take place. In many cases such regions determine the nature of the collision process. Therefore, the above, very useful criterion must be applied cautiously. [*See* COLLISION CROSS SECTIONS (ATOMIC PHYSICS).]

B. Cross Section Defined

The effect of atomic particles on each other is generally described via an interaction cross section. The conceptually simplest cross section,

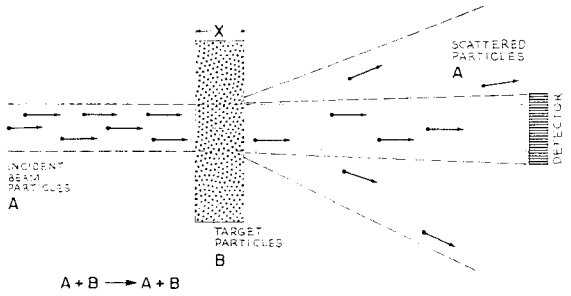

FIG. 1. Beam experiment to obtain the scattering cross section of A by particles B. [From Johnson, R. E. (1982). *Introduction to Atomic and Molecular Collisions*. Plenum Press, New York.]

the total collision cross section, is obtained from an experiment like that in Fig. 1. A beam of particles is incident on a target containing atoms, and the change in intensity of the beam is monitored. If the target is "thin" so that an incident particle is only likely to make a single collision, then the change in intensity, ΔI, for a small change in thickness, Δx, is written

$$\Delta I = -\sigma n_B I \, \Delta x \tag{1}$$

where n is the density of target atoms and I is the measured intensity (particles/cm^2/sec). In Eq. (1) the proportionality constant σ is the cross section, indicating, roughly, the range of the interaction between the colliding particles. Integrating Eq. (1), the intensity of unscattered particles versus thickness x can be found for thick samples:

$$I = I_0 e^{-n_B \sigma x} \tag{2}$$

Differentiating I in Eq. (2), the quantity $dI/I_0 = (n_B\sigma)e^{-n_B\sigma x}\,dx$ is the Poisson probability of the first collision occurring between x and $x + dx$, and $(n_B\sigma)^{-1}$ is called the mean free path between collisions.

One of the first results found from such measurements is that the total cross section varies slowly with velocity as shown in Fig. 2. That is, atoms have diffuse boundaries and the effective range of the interaction region changes with velocity. This dependence is wave mechanical in nature, as the cross section is determined by the amount of scattering at small angles, which is the diffraction region mentioned above. Total cross sections that are calculated strictly classically from *realistic* potentials are always infinite. Hence, we see in this simplest of examples the need for cross-section approximations that incorporate wave-mechanical effects.

A second set of experiments for studying

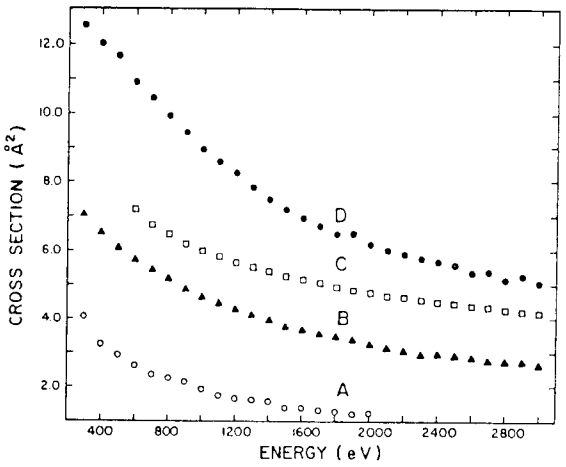

FIG. 2. He + He. Detector apertures: A 0.57°, B 0.26°, C 0.11°, D 0.056°. [From W. J. Savola, Jr., F. J. Erikssen, and E. Pollack (1973). *Phys. Rev.* **A7**, 932.]

atomic interactions requires detection of those particles that are scattered rather than those not scattered. For a beam of atoms A incident on a target containing atoms B, the angular differential cross section

$$d\sigma = (d\sigma/d\Omega)_A \, d\Omega$$

relates the number of incident particles per unit time scattered into a region of solid angle $d\Omega$ to the incident flux. Similarly,

$$d\sigma = (d\sigma/d\Omega)_B \, d\Omega$$

relates the number of target particles per unit time ejected into a region of solid angle to the flux of incident particles. Of course, collecting all particles A scattered into all solid angles is equivalent to detecting all scattered particles. Hence, integrating $d\sigma$ over all angles yields the total scattering cross section σ described above. In the experiment described, one might also discriminate between any internal changes that have occurred (e.g., changes in mass, charge, energy, etc.) The cross sections determined from such an experiment, therefore, would indicate both the nature of the interaction between A and B and the likelihood of an internal change (transition) in either A or B. These two aspects of the cross section will be brought out more clearly in the subsequent discussion. When no internal changes occur the collisions are called elastic; when such changes occur we refer to them as inelastic.

In this chapter we first elaborate on the nature of the cross section using a semiclassical description referred to as the impact parameter method. We then discuss the forces between atomic particles and subsequently use those forces to calculate cross sections and transition probabilities. Such calculations are divided into those methods useful for transitions in fast collisions and those useful in slow collisions. For incident ions and atoms, collisions are fast or slow depending on whether the ratio τ_c/τ_0 is less than or greater than 1. Here τ_c is the collision time ($\sim d/v$, where d is a characteristic dimension associated with A and B, e.g., $d \approx a_0$ for outer shell electrons, and v is the relative speed) and τ_0 is the characteristic period of the system of particles. For ionization of outer-shell electrons, the characteristic period is $\tau_0 \approx 10^{-16}$–10^{-17} sec, whereas for molecular processes, $\tau_0 \approx 10^{-14}$ sec for vibrational motion and $\tau_0 \approx 10^{-13}$ for rotational motion. Setting $\tau_c \approx \tau_0$, such characteristic times translate into incident-particle energies of the order 1–100 keV/amu, 0.1 eV/amu, and 0.001 eV/amu, where amu is the atomic mass unit. When $\tau_c/\tau_0 \approx 1$, the collision time is about the same size as the characteristic period and the transition probabilities and cross sections are large. At much larger or much smaller times, the cross sections are found to decrease.

As the interaction between even the simplest atoms can be quite complex, many of the details of the following discussion are treated qualitatively. The purpose of the presentation following is to let the reader have a "feel" for the complexities and yet acquire the ability to understand the nature of the approximate expressions and formulas used by many workers in the field of atomic and molecular collisions. The discussion starts using the classical impact parameter concept to formulate cross sections of various types so the reader has a clear idea of the definitions of the quantities calculated and used later.

II. Impact Parameter Cross Sections

A. Formulation

The trajectory of an incident particle A interacting repulsively with an initially *stationary* target particle B is shown in Fig. 3. The quantity b in that figure indicates the closeness of approach and is referred to as the impact parameter. It is the perpendicular distance between the incident velocity vector $\mathbf{v}$ and the position $\mathbf{R}$ of particle A measured from B. The impact parameter also indicates the angular momemtum of the colliding particles (i.e., $|L| = |M_A\mathbf{R} \times \mathbf{v}| = M_A v b$). The

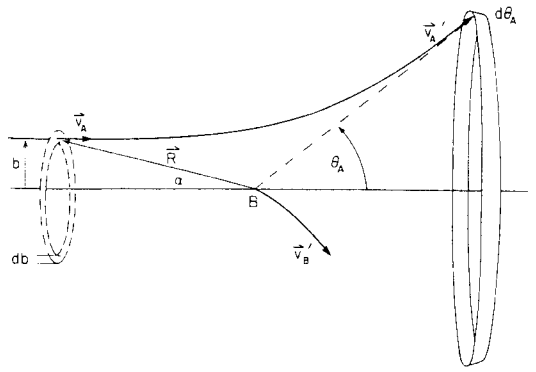

FIG. 3. Scattering of A by B: b is impact parameter, **R** shows initial position of A with respect to B, $\mathbf{v}_A$ is the initial velocity, $\mathbf{v}_A'$ and $\mathbf{v}_B'$ are the final velocities, and θ_A is the scattering angle for A: $\mathbf{v}_A = \mathbf{v}$ here.

impact parameter (or angular momentum) and the relative velocity v (or energy) are sufficient to characterize collisions between spherically symmetric particles. As the impact parameter between two colliding particles determines the likelihood of a deflection, we assign a collision probability $P_c(b, v)$ for each impact parameter. If the incident and/or target particle has a spin or is a molecule, then initial orientations with respect to the collision axis have to be specified, for example, $P_c(b, \phi, \omega, v)$ where ϕ is the azimuthal angle of approach and ω is an orientation angle. However, if there are no preferential aligning fields (e.g., outside fields or target B in a crystalline lattice), then the incident and target particles are presumed to be randomly oriented and $P_c(b, v)$ is an average over collisions involving all possible orientations.

Based on the experimental definition in Eq. (1), the interaction cross section between A and B can now be written

$$\sigma(v) = 2\pi \int_0^\infty P_c(b, v) b \, db \tag{3}$$

That is, the particles passing through the ring of area $2\pi b \, db$ about a single target atom, (e.g., Fig. 3) will be scattered from the beam with a probability P_c and, hence, contribute to the observed change in intensity of the beam, ΔI in Eq. (1). In classical mechanics, processes are deterministic and hence, P_c is either 0 or 1. For a finite-range interaction (e.g., collision between two spheres of radius r_A and r_B), $P_c = 0$ for $b > r_A + r_B$ and the cross section is finite, $\sigma = \pi(r_A + r_B)^2$. For interactions between atomic or molecular particles the forces are infinite in range (i.e., $P_c = 1$ for all b) yielding a classical cross section which is infinite. Quantum mechanics, on the other hand, gives finite cross sections for most realistic interactions, like the measured values in Fig. 2. That is, $P_c(b, v) \xrightarrow{b\to\infty} 0$ in a quantum-mechanical calculation for interactions that decay rapidly at large separation. This deficiency in the classical estimate of the cross section may not be of practical importance in many applications. That is, one generally wants to know whether a particle experiences a deflection or loses an amount of energy larger than some prescribed minimum size and *not* the likelihood of being deflected even at infinitesimally small angles (i.e., extremely large b).

From Fig. 3 it is seen that if the forces between the particles are independent of their orientations (i.e., no azimuthal dependence), then those particles passing through the ring of area $2\pi b \, db$ will be scattered into an angular region $2\pi \sin\theta_A \, d\theta_A$. Therefore

$$d\sigma = (d\sigma/d\Omega)_A 2\pi \sin\theta_A \, d\theta_A = 2\pi b \, db$$

so that the differential cross section discussed earlier is

$$\left(\frac{d\sigma}{d\Omega}\right)_A \equiv \sigma(\theta_A) = \left|\frac{b \, db}{\sin\theta_A \, d\theta_A}\right| \tag{4a}$$

where the simplified notation for azimuthally symmetric cross section, $\sigma(\theta_A)$, is often used instead of $(d\sigma/d\Omega)_A$. Similarly, the cross section for scattering of target particles is

$$\left(\frac{d\sigma}{d\Omega}\right)_B \equiv \sigma(\theta_B) = \left|\frac{b \, db}{\sin\theta_B \, d\theta_B}\right| \tag{4b}$$

For an elastic binary collision of the type we have been discussing, the energy and momentum of each particle after the collision can be related to the incident energy and the scattering angle using the conservation of energy and momentum. The scattering angle can be expressed either in the laboratory or in the center of mass (CM) system. In a practical problem the former is more useful, but in describing the relationship between the atomic interactions and the resulting deflections the latter is much more convenient. In Table I the relationships between laboratory and CM quantities are summarized for the case we have been discussing, a moving particle A incident on a stationary particle B. We write the CM deflection angle versus b as $\chi(b)$ (the deflection function) and, therefore, by analogy with the above discussion, the classical differential cross section in the CM system is

$$\sigma(\chi) = \left|\frac{b \, db}{\sin\chi \, d\chi}\right| \tag{5}$$

TABLE I. Relationship between Laboratory and CM Variables

Velocity of CM	$\mathbf{V}_c = (M_A\mathbf{v}_A + M_B\mathbf{v}_B)/(M_A + M_B) \equiv \dot{\mathbf{R}}_c$
Relative velocity in CM	$\mathbf{v} = (\mathbf{v}_A - \mathbf{v}_B) \equiv \dot{\mathbf{R}}$

Total laboratory quantities	CM quantities
$M = M_A + M_B$	$m = M_AM_B/(M_A + M_B)$
$E_A + E_B = \frac{1}{2}MV_c^2 + E$	$E = \frac{1}{2}mv^2$
$\mathscr{P} = M\mathbf{V}_c$	$\mathbf{P} = 0$
$\mathscr{L} = M\mathbf{R}_c \times \mathbf{V}_c + \mathbf{L}$	$\mathbf{L} = m\mathbf{R} \times \mathbf{v}$

Transformations (for v_B initially zero and elastic collisions):

$$\theta_B = \tfrac{1}{2}(\pi - \chi)$$

$$\tan\theta_A = \mu \sin\chi/(1 + \mu\cos\chi); \qquad \mu = M_B/M_A$$

$$T = \gamma E_A \sin^2(\chi/2); \qquad \gamma = 4M_BM_A/(M_A + M_B)^2$$

$$(d\sigma/d\Omega)_A = \sigma(\chi)\left|\frac{d\cos\chi}{d\cos\theta_A}\right| = \sigma(\chi)\frac{(\mu^2 + 2\mu\cos\chi + 1)^{3/2}}{\mu^2|\mu + \cos\chi|}$$

$$(d\sigma/d\Omega)_B = \sigma(\chi)\left|\frac{d\cos\chi}{d\cos\theta_B}\right| = \sigma(\chi)|4\sin(\chi/2)|$$

$$\frac{d\sigma}{dT} = \frac{4\pi}{\gamma E_A}\sigma(\chi)$$

This can be transformed (see Table I) to give the laboratory scattering cross sections in Eqs. (4) for the incident or target particle.

B. Energy Loss Cross Sections

For elastic collisions the energy transfer to B is simply related to χ when B is initially stopped (see Table I) and, therefore, it is often useful to consider the elastic energy transfer cross section instead of $\sigma(\chi)$. Calling T the energy transfer to particle B, one writes

$$\frac{d\sigma}{dT} = \frac{4\pi}{\gamma E_A}\sigma(\chi) \tag{6}$$

where γ is given in Table I. The reader will find both $\sigma(\chi)$ and $d\sigma/dT$ used in the literature and, therefore, should keep in mind that they are related. In addition to transferring kinetic energy T to particle B, there is also a probability that one or both particles will experience a change in internal energy (a transition), which we label $P_{0\to f}(b, v)$. The subscripts indicate the initial (0) and final (f) states of the colliding particles, and those collisions for which $P_{0\to f} \neq 0$ are inelastic. As in Eq. (3), an *inelastic* cross section can be written

$$\sigma_{0\to f}(v) = 2\pi\int_0^\infty P_{0\to f}(b, v)b\,db \tag{7}$$

As each inelastic process is associated with an internal energy change $Q_{0\to f}$, the average inelastic energy lost to such processes is

$$\bar{Q}(b) = \sum_f Q_{0\to f}P_{0\to f}(b, v) \tag{8}$$

In writing Eq. (8) we assumed the sum of probabilities over all processes, including no internal energy change, is unity [$\sum_f P_{0\to f} = P_c(b, v) = 1$]. [*See* COLLISION-INDUCED SPECTROSCOPY.]

We can use the above to define the average energy loss per unit path length for particle A traversing a material consisting of particles B. In passing through a target, A loses energy both to electronic excitations and to kinetic energy transfer to target nuclei B. Noting that $(n_B\sigma_{0\to f})^{-1}$ is the mean free path for the occurrence of an energy loss $Q_{0\to f}$, the averaged electronic energy loss per unit path length in the target is

$$\left(\frac{dE}{dx}\right)_e = \sum_f Q_{0\to f}(n_B\sigma_{0\to f}) \tag{9}$$

Similarly, if $[n_B(d\sigma/dT)\,dT]^{-1}$ is the mean free path for losing an amount of kinetic energy between T and $T + dT$ to a nucleus B, then the averaged elastic loss of A *per unit path length* in

the target is

$$\left(\frac{dE}{dx}\right)_n = \int_0^\infty T[n_B(d\sigma/dT)dT] \qquad (10)$$

To the extent that the excitations and collisional energy transfers are independent, the average net energy loss is the sum of these. Because they both depend on the material number density, this is generally written

$$\left(\frac{dE}{dx}\right) = n_B(S_e + S_n) \qquad (11)$$

with

$$S_e = \sum Q_{0\to f}\,\sigma_{0\to f} = 2\pi \int_0^\infty Q(b)b\,db \qquad (12a)$$

$$S_n = \int_0^\infty T\left(\frac{d\sigma}{dT}\right) dT = 2\pi \int_0^\infty T(b)b\,db \qquad (12b)$$

The quantity (dE/dx), which has been measured extensively, is referred to as the stopping power of the material, and the quantities S_e and S_n are the electronic and nuclear elastic stopping cross sections. These are quantities determined only by the single collision interaction of A with B and not properties of the target as a whole. Results for S_e are tabulated, and simple, generally useful expressions for S_n are available, for example, see Table II.

The nuclear stopping cross section S_n is related to another useful quantity, the diffusion cross section σ_d. The change in the parallel com-

TABLE II. Elastic Collision Expressions

$$\chi(b) = \pi - 2b\int_{R_0}^\infty \frac{dR}{R^2}\left(1 - \frac{b^2}{R^2} - \frac{V}{E}\right)^{-1/2}$$

$$\approx -\left(\frac{1}{2E}\right)\frac{d}{db}\int_{-\infty}^\infty V(R)\,dZ$$

$$\eta^{sc}(b) = \frac{p_0}{\hbar}\left[\int_{R_0}^\infty \left(1 - \frac{b^2}{R^2} - \frac{V}{E}\right)^{1/2} dR - \int_b^\infty \left(1 - \frac{b^2}{R^2}\right)^{1/2} dR\right] \approx \frac{-1}{2\hbar v}\int_{-\infty}^\infty V(R)\,dZ$$

$$L\chi(b) = (2\hbar b)\frac{\partial \eta^{sc}(b)}{\partial b}, \qquad L = p_0 b = mvb$$

$$\sigma(\chi) = \frac{\gamma E_A}{4\pi}\frac{d\sigma}{dT} \quad (B \text{ initially stopped}), \qquad S_n = \frac{\gamma E_A}{2}\sigma_d$$

$$\rho = \chi \sin\chi\sigma(\chi), \qquad \tau = \chi E,\ E = \frac{M_B}{M_A + M_B}E_A$$

Quadratures (m = number of integration points)

$$g(x) \equiv \frac{b}{R_0}\left[\frac{1 - x^2}{1 - (b/R_0)^2x^2 - \dfrac{V(R_0/x)}{E}}\right]^{1/2}$$

$$\chi(b) \approx \pi\left[1 - \frac{1}{m}\sum_{i=1}^m g(x_i)\right],$$

$$x_i = \cos[(2i - 1)\pi/4m]$$

$$\eta^{sc}(b) \approx \frac{2L}{\hbar}\left\{\frac{\pi}{(2m + 1)}\sum_{j=1}^m \sin^2\left(\frac{j\pi}{2m + 1}\right)[g(x_j)^{-1} - 1]\right\},$$

$$x_j = \cos\left[\frac{j\pi}{2m + 1}\right]$$

(continues)

TABLE II. *(Continued)*

Impulse estimates ($V/E \ll 1$)

for $V = C_n/R^n$, $\quad \chi(b) \approx a_n V(b)/E$,

$$a_n = \pi^{1/2}\Gamma\left(\frac{n+1}{2}\right)/\Gamma\left(\frac{n}{2}\right) \xrightarrow{n\to\infty} (\pi n/2)^{1/2}$$

$$\eta^{sc}(b) \approx \frac{-L\chi(b)}{2\hbar(n-1)}$$

[$\Gamma(x+1) = x\Gamma(x)$, $\Gamma(1) = 1$, $\Gamma(\frac{1}{2}) = \pi^{1/2}$; gamma function tabulated]

$$\rho \approx n^{-1}(a_n C_n/\tau)^{2/n}$$

$$\frac{d\sigma}{dT} \approx \frac{\pi}{n}\mathcal{A}_n^2/(\gamma E_A)^{1/n}T^{1+1/n};\ \mathcal{A}_n = \left(\frac{2M_A}{M_A+M_B}a_n C_n\right)^{1/n}$$

$$S_n \approx \frac{\pi}{n-1}\mathcal{A}_n^2(\gamma E_A)^{1-2/n},\ n > 2$$

for $V = (Z_A Z_B e^2)\exp(-\beta R)/R$

$$\chi(b) \approx \frac{(Z_A Z_B e^2)\beta}{E}K_1(\beta b) \xrightarrow{b\to\infty} \left(\frac{\pi\beta b}{2}\right)^{1/2}\frac{V(b)}{E}$$

$$\eta^{sc}(b) \approx -\frac{(Z_A Z_B e^2)}{\hbar v}K_0(\beta b) \xrightarrow{b\to\infty} \frac{-L\chi(b)}{2\hbar(\beta b)}$$

(K_n are the modified Bessel functions; tabulated)

Massey–Mohr [Eq. (31)]

$$\sigma \approx 2\pi(\bar{b})^2\left(1+\frac{1}{2n-4}\right) \qquad (n > 2)$$

$$\bar{b} \approx \left[\frac{2a_n C_n}{(n-1)\hbar v}\right]^{1/(n-1)}$$

Born approximation

for $V = (Z_A Z_B e^2)\exp(-\beta R)/R$

$$\frac{d\sigma}{dT} \approx \pi\mathcal{A}^2/(\gamma E_A)(T+T_0)^2$$

$$\mathcal{A} = \left(\frac{2M_A}{M_A M_B}Z_A Z_B e^2\right)$$

$$T_0 = \frac{(\hbar\beta)^2}{2M_B}$$

$$\sigma \approx \pi\mathcal{A}^2/T_0(\gamma E_A + T_0)$$

$$S_n \approx \frac{\pi\mathcal{A}^2}{(\gamma E_A)}\left[\ln\left(\frac{\gamma E_A}{T_0}+1\right) - \frac{\gamma E_A}{(\gamma E_A + T_0)}\right]$$

Thomas–Fermi (Lindhard)

Scaling quantities

$$a_{TF} = 0.8853 a_0/(Z_A^{2/3} + Z_B^{2/3})^{1/2}$$

$$\varepsilon = (\gamma E_A)a_{TF}/2\mathcal{A}, \qquad \mathcal{A} \text{ as above}$$

$$t = \varepsilon^2 T/(\gamma E_A)$$

$$\frac{d\sigma}{dt} \approx \pi a_{TF}^2\xi/4t^{4/3}[1+\xi^{2/3}t^{4/9}]^{3/2}, \qquad \xi \approx 2.62$$

$$S_n \approx \left(\frac{9\pi}{2}\right)\frac{\mathcal{A}^2}{(\gamma E_A)}\{\ln[\mathcal{B}+(1+\mathcal{B}^2)^{1/2}] - \mathcal{B}/(1+\mathcal{B}^2)^{1/2}\}$$

$$\mathcal{B} = \xi^{1/3}\varepsilon^{4/9}$$

(continues)

TABLE II. (*Continued*)

Lenz–Jensen potential

$$V = \frac{Z_A Z_B e^2}{R}\,\Phi(R/a_{TF})$$

$$\Phi = (1 + b_1 y + b_2 y^2 + b_3 y^3 + b_4 y^4)e^{-y}$$

$$y = (9.67R/a_{TF})^{1/2}, \qquad b_1 = 1, \qquad b_2 = 0.3344$$

$$b_3 = 0.0485, \qquad b_4 = 0.002647$$

ponent of momentum of a very slow particle A due to a collision with B involving no electronic excitations is written $(\Delta \mathbf{p}_a)_{//} = p_0\,(1 - \cos\chi)$. Therefore, the drag force on a particle A traversing a target containing particles B is the collision rate times this momentum loss,

$$(\Delta \mathbf{F}_A)_{//} = \int (\Delta \mathbf{p}_A)_{//}\, v n_B\, (2\pi b\, db)$$

This can be written as $(\Delta \mathbf{F}_A)_{//} = n_B p_0 v \sigma_d$, where

$$\sigma_d = 2\pi \int_0^\infty [1 - \cos\chi(b)]\, b\, db$$

$$= 2\pi \int_{-1}^{1} (1 - \cos\chi)\sigma(\chi)\, d(\cos\chi) \quad (13)$$

Using the expression for T given in Table I we see that S_n and σ_d are related:

$$S_n = \frac{\gamma E_A}{2}\,\sigma_d \quad (14)$$

That is, the drag force on a particle is related to the stopping power, i.e., $(\Delta \mathbf{F}_A)_{//} = (1 + \mu)\,(dE/dx)_n$, where $\mu = M_B/M_A$. Because the factor $(1 - \cos\chi)$ goes to zero as χ goes to zero, both S_n and σ_d, unlike σ, can be calculated classically, as we will see later.

We have defined a number of cross sections in the above discussion. These are all described without references to the forces between the particles. These forces produce both the deflections and the transitions (inelastic processes) discussed above. However, it has become customary to separate the discussion of these two effects. We follow this tradition here and consider first the calculation of deflections for two spherically symmetric colliding particles.

III. Elastic Scattering

A. Classical Deflection Function

The determination of $\chi(b)$, the CM deflection function, begins with angular momentum conservation. In the CM system the two colliding particles follow trajectories that are equivalent and the collision can be described as the scattering of a particle of reduced mass m by a stationary center of force. Using the coordinates given in Fig. 3. we write the angular momentum as

$$L = mvb = mR^2\dot{\alpha} \quad (15)$$

Rearranging Eq. (15) and integrating over time, we obtain

$$\chi(b) = \pi - \int_{-\infty}^{\infty} \dot{\alpha}\, dt = \pi - vb \int_{-\infty}^{\infty} \frac{dt}{R^2}$$

Finally, assuming an interaction potential $V(R)$ that depends only on the separation R, energy conservation is expressed as

$$\frac{1}{2} m\dot{R}^2 + \frac{L^2}{2mR^2} + V(R) = E$$

Employing Eq. (15), this expression can be written as a radial velocity,

$$\dot{R} = \pm v \left[1 - \frac{b^2}{R^2} - \frac{V}{E}\right]^{1/2} \quad (16)$$

At the start of the collision the radial velocity is $(-v)$, that is, the atoms approach each other at a speed v. As R decreases, $\dot{R}$ approaches zero. R then begins to increase, as the particles recede, until it becomes $(+v)$ at large separations. Using Eq. (16) the deflection function above can be written

$$\chi(b) = \pi - 2b \int_{R_0}^{\infty} \frac{dR}{R^2} \left[1 - \frac{b^2}{R^2} - \frac{V}{E}\right]^{-1/2} \quad (17)$$

where R_0 is the distance of closest approach at which $\dot{R} = 0$. This expression can be integrated analytically for a few potentials of the form $V(R) = C_n/R^n$ but otherwise is treated by a simple numerical procedure given in Table II.

B. Impulse Approximation

For fast incident ions [ratio V/E small for all R in Eq. (17)] the deflections are small and it is useful to replace the above expressions for $\chi(b)$

by an impulse approximation. That is,

$$\chi(b) = \frac{(\Delta p)_\perp}{p_0} \approx \frac{\int_{-\infty}^{\infty} F_\perp \, dt}{p_0}$$

$$= -\frac{d}{db}\left[\frac{1}{2E}\int_{-\infty}^{\infty} V \, dZ\right] \qquad (18)$$

In this equation we assumed a straight line trajectory, i.e., $R^2 \approx b^2 + Z^2$, with $Z = vt$. For the general class of power-law potentials ($V = C_n/R^n$), $\chi(b)$ calculated from Eq. (18) is given in Table II. It is seen, that the deflection is determined primarily by the nature of the potential *near the distance of closest approach* of the colliding particles ($R_0 \approx b$). Therefore, it is *not* necessary to know the potential accurately at all R to obtain a reasonable estimate of the deflection function for collisions between ions and atoms as long as $V/E \ll 1$. Since V is of the order of electron-volts, this criterion is satisfied for a large number of problems involving incident ions, atoms, or molecules.

From Eq. (18) the quantity $\tau = \chi E$ (which in the laboratory frame is $\tau \approx \theta_A E_A$ for small angles) is seen to depend only on the impact parameter. Also, the modified cross section $\rho = \chi(\sin\chi)\,\sigma(\chi)$ [in the lab frame, $\theta_A \sin\theta_A \sigma(\theta_A)$] obtained using Eq. (18) in Eq. (5), is *independent of the energy E* for small angles (Table II). Based on these results, experimental measurements of ρ versus τ can be directly converted into power-law potentials that are applicable over limited ranges of R. It is seen in Fig. 4 that for colliding atoms, $n \to 1$ as $R_0 \to 0$ (i.e., τ gets large). That is, the interaction is the repulsive interaction between the nuclei. As R_0 increases (τ decreases), n increases, reflecting the electron screening of the repulsive interaction. Because of the simplicity of the power potential results, they are used frequently to calculate effects of energetic charged particles incident on solids for which knowledge of the potential is only needed over a limited range of interaction radii.

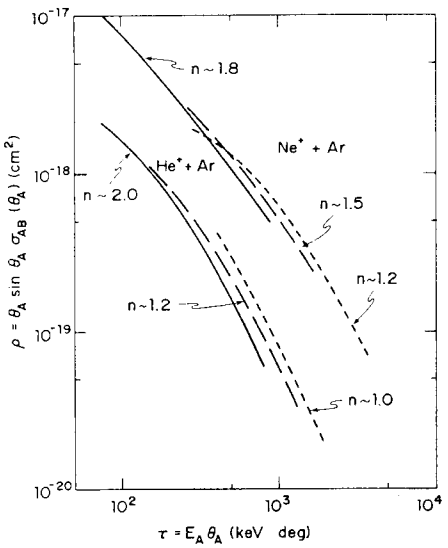

FIG. 4. Values of ρ versus τ experiment for three values of E_A: ——— 25 keV; — — — 50 keV; – – – 100 keV. Approximate power laws indicated by n. [Data from E. N. Fuls, P. R. Jones, F. P. Ziemba, and E. Everhart (1957). *Phys. Rev.* **107,** 104. Figure from R. E. Johnson (1982). "Introduction to Atomic and Molecular Collisions." Plenum Press, New York.]

Before discussing the determination of interaction potentials for specific collision pairs, we examine the nature of differential cross section for two forms of the potential, a purely repulsive and a long-range attractive plus short-range repulsive potential. The latter potential is characteristic of the interaction of an ion with an atom or molecule in its ground state. In Fig. 5 are shown the deflection functions and ρ versus τ plots. Based on Table II it is clear that the deflection function should approximately follow the form of the potential. Therefore, for the repulsive potential shown, χ is always positive, attaining a maximum value of π for head-on collisions [$b = 0$, Eq. (17)]. For the other potential, χ is negative at large b, eventually becomes positive, and again reaches π at $b = 0$. However, χ goes through a minimum, χ_r, at the impact parameter labeled b_r. At this minimum, $d\chi/db = 0$, and, therefore, the classical calculation of cross section in Eq. (5) becomes *infinite*. This large

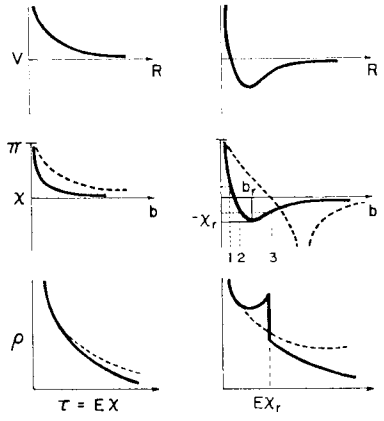

FIG. 5. Values of χ versus b and ρ versus τ for a repulsive and an attractive potential. Rainbow angle and impact parameter are χ_r and b_r. Three impact parameter's contribution for $|\chi| < |\chi_r|$ are labeled. Solid line higher energy, dashed line low energy. [From R. E. Johnson (1982). "Introduction to Atomic and Molecular Collisions," p. 53. Plenum Press, New York.]

enhancement in the scattering probability is similar to the effect that produces rainbows in the scattering of light from water droplets; hence, χ_r is called the rainbow angle. When $\chi_r < \pi$, then for angles greater than χ_r, only one impact parameter contributes to the cross section. However, for angles less than χ_r, three impact parameters contribute that have the same value of $\cos \chi$.

Using a Lennard–Jones form for the long-range attractive plus short-range repulsive potential, $V = C_{2n}/R^{2n} - C_n/R^n$, and for the power-law results in Table II the rainbow angle (for $V \ll E$) is

$$\chi_r \approx \frac{a_n^2}{a_{2n}} \left(\frac{V_{\min}}{E}\right) \tag{19}$$

That is, the rainbow angle is determined by the depth of the potential minimum $V_{\min}$ (which is $V_{\min} = -C_n^2/4C_{2n}$ for the Lennard–Jones potential), and the shape of the potential via a_n and a_{2n}. Because the ratio a_n^2/a_{2n} changes slowly with n, measuring the rainbow angle can directly give an estimate of potential well depth.

As the collision energy decreases, χ_r can become much larger than π, implying that the two particles may orbit each other before separating. In fact, for very small velocities there is a particular impact parameter for which the particles can be trapped in orbit (i.e., $\ddot{R} = 0$ at $\dot{R} = 0$). Using only the attractive part of potential, along with Eq. (16) and the power-low results in Table II, the orbiting impact parameter is

$$b_0 \approx \left[\left(\frac{n}{2}\right)\frac{C_n}{E}\right]^{1/n} \Big/ \left(\frac{n-2}{n}\right)^{(n-2)/2n} \tag{20}$$

Therefore, for $b \leq b_0$, the interaction times can be very long and the particles approach each other closely, whereas for $b > b_0$ the particles simply scatter. This fact has been used extensively in estimating ion–molecule interaction cross sections [see Section VI,H].

Near the rainbow angle (or when orbiting occurs), a number of impact parameters contribute to the scattered flux at a given observation angle; hence, interference phenomena occur and classical cross-section estimates are not valid. However, if the angular resolution is not large the simple addition of the contribution to the scattered flux from each impact parameter gives an adequate representation of the cross section. This was used to give ρ versus τ in Fig. (5). That is,

$$\sigma(\chi) \approx \sum_i \left|\frac{b\,db}{\sin\chi\,d\chi}\right|_{b=b_i} \tag{21}$$

where the b_i are all those impact parameters giving the same value of $\cos\chi$ [i.e., $\chi \to \pm(\chi + 2\pi m)$, m an integer]. As the interference phenomenon can give important additional information about the *details* of the interaction potentials, wave-mechanical calculations are useful. In addition, the effects at very small angles and at low energies can only be described via wave mechanics. In the following, therefore, we briefly review that wave-mechanical description of the elastic scattering cross section that parallels the above discussion. We thereby obtain results for diffraction (e.g., total cross sections σ) and interference (e.g., rainbow) phenomena. The results have parallels in light scattering.

IV. Wave Mechanics of Scattering

A. The Scattering Amplitude

In wave mechanics the scattering of the particle is replaced by scattering of a wave, but here again we can describe this scattering in the CM system, as the transformation between the laboratory and CM quantities is the same as in Table I. The beam of particles incident on a target is replaced by a plane wave, $\exp(i\mathbf{K}\cdot\mathbf{R} - i\omega t)$, where $\hbar\mathbf{K}$ replaces the momentum and $\hbar\omega = \hbar^2K^2/2m$ is the energy per particle in the beam. K^{-1} is often written as $\lambda\!\!\!^{-}$ where $\lambda\!\!\!^{-} = \lambda/2\pi$, with λ the wavelength. Describing the beam of particles as a plane wave implies that the particles are nonlocalized, that is, it is equally probable to find a particle at any point in the beam. When this wave is scattered, as in light scattering, the outgoing wave at very large distances from the scattering center has the form

$$\left[\exp(i\mathbf{K}\cdot\mathbf{R}) + f(\chi)\frac{e^{iKR}}{R}\right] e^{-i\omega t} \tag{22}$$

where we have assumed, as in the above discussions, spherical scattering centers (i.e., no azimuthal dependence). The magnitude of the scattered wave in an angular region about χ is given by $|f(\chi)|^2/R^2$ in Eq. (22), where $f(\chi)$ is referred to as the scattering amplitude and R is the distance from the scattering center. The plane wave in Eq. (22) is the unscattered portion of the wave, which is assigned unit amplitude. This implies that the scattering potential is only a small disturbance. The differential cross section (probability of scattering into a unit solid angle about χ) is simply

$$\sigma(\chi) = |f(\chi)|^2 \tag{23}$$

Therefore, the scattering problem reduces to solving the Schroedinger wave equation subject to the boundary condition at large R, which is expressed by the form of the wave function in Eq. (22).

To draw analogies with the classical calculation of cross section, it is customary to express the plane wave in terms of multipole moments,

$$\exp(i\mathbf{K}\cdot\mathbf{R}) = \sum_{l=0}^{\infty} i^l(2l+1)P_l(\cos\chi)j_l(KR)$$

The $j_l(KR)$ are the spherical Bessel functions, which have the asymptotic form, as $R \to \infty$

$$j_l(KR) \to \frac{\sin(KR - l\pi/2)}{KR}$$

The P_l are the Legendre polynomials, where l labels the various moments ($l = 0$, spherical; $l = 1$, dipole; $l = 2$, quadrupole; etc.). In the present problem, however, l also is the angular momentum index [$L^2 = l(l+1)\hbar^2$]. Therefore, l replaces the impact parameter b, which we used in the classical description

$$b \to \sqrt{l(l+1)}\,\hbar/mv \approx (l+\tfrac{1}{2})/K = (l+\tfrac{1}{2})\lambda\!\!\!^{-} \tag{24}$$

Upon intersecting a scattering center, each spherical wave j_l experiences a phase shift (η_l), becoming $\sin(KR - l\pi/2 + \eta_l)/KR$ in the asymptotic region. Therefore, one can use these expressions to write

$$f(\chi) = \frac{1}{2Ki} \times \sum_{l=0}^{\infty}(2l+1)\,[\exp(2i\eta_l) - 1]\,P_l(\cos\chi) \tag{25}$$

Substituting Eq. (25) into Eq. (23) indicates that the *determination of the scattering cross section* reduces to the *determination of the phase shifts*. Before calculating η_l we use the form for $f(\chi)$ in Eq. (25).

The total cross section, obtained by integrating over the angle in Eq. (23), becomes

$$\sigma = 2\pi\int_{-1}^{1}|f(\chi)|^2\,d(\cos\chi) = \frac{8\pi}{K^2}\sum_{l=0}^{\infty}(l+\tfrac{1}{2})\sin^2\eta_l \tag{26}$$

If the phase shifts are zero, no scattering has occurred and the cross section is zero. Further, for large-momentum collisions (small wavelengths) the sum in l above can be approximated by an integral in b using Eq. (24). The expression for σ can then be written in the same form as the classical cross section in Eq. (3) if we define $P_c(b) \approx 4\sin^2\eta(b)$. (Here the dependence of the phase shift η on l is written as a dependence on b.) This expression for P_c clearly demonstrates that at large impact parameters (or l) when $\eta(b)$ goes to zero the wave-mechanical scattering probability $P_c(b)$ goes to zero.

Comparing Eqs. (25) and (26), it is also seen that

$$\sigma = \frac{4\pi}{K}\,\mathrm{Im}\,f(0) \tag{27}$$

This result is referred to as the optical theorem, based on analogy with light scattering, and it shows directly what we stated much earlier. The cross section σ is determined by scattering at zero degrees, which for wave scattering is a diffraction region. Note also that the probability P_c above has an average value of 2 at small b and not unity as it is classically. These facts both emphasize that the total scattering cross section σ is a nonclassical quantity. Note that, although the sum in Eq. (25) can also be replaced by an integral over b at small wavelengths, the expression for differential cross section so obtained is quite *different* from the classical expression in Eq. (21). That is, in wave mechanics the *scattering amplitudes* for each impact parameter (or l) that contribute to scattering at angle χ are added, whereas classically the *cross sections* that contribute at angle χ are added [e.g., Eq. (21)]. Hence, the wave-mechanical cross section can exhibit an *oscillatory* behavior.

B. Semiclassical Cross Section

The relationship between the classical and wave-mechanical cross sections becomes clearer if the sum in Eq. (25) is examined in more detail. At those impact parameters b_i producing classical scattering into the angular region χ, *constructive interference* occurs in the sum in Eq. (25). Therefore, the classical trajectories are like the light rays in geometrical optics. The angular differential cross section

$$\sigma(\chi) = |f(\chi)|^2 \approx \left|\sum_i \sigma[\chi(b_i)]^{1/2}\exp[i\alpha(b_i)]\right|^2 \tag{28}$$

replaces the classical expression in Eq. (21), where the $\sigma[\chi(b_i)]$ are the classical cross sections, $|b\,db/\sin\chi\,d\chi|_{b=b_i}$, used in Eq. (21). Equation (28) directly exhibits the interference between contributions from different impact pa-

rameters. In this expression the phase factor is $\alpha(b) = A/\hbar \pm \varepsilon$, where ε is a multiple of $\pi/4$. Here A is the difference in the classical action between an undeflected particle and a scattered particle, $A = 2\hbar\eta^{sc}(b) - L\chi$ with

$$\hbar\eta^{sc}(b) = \int_{R_0}^{\infty} p(R)\, dR - \int_{b}^{\infty} p_0(R)\, dR$$

The regions of constructive interference are those for which the *classical action is a minimum* ($\partial A/\partial b = 0$), so that

$$\chi = \left(\frac{2}{K}\right)\frac{\partial\eta^{sc}(b)}{\partial b} \tag{29}$$

On substituting the form for $\eta^{sc}(b)$ given above, Eq. (29) becomes equivalent to the expression for $\chi(b)$ in Eq. (17). Therefore, each region of constructive interference corresponds to a classical trajectory that contributes at angle χ. If only one impact parameter contributes in Eq. (28), the semiclassical result for $\sigma(\chi)$ is *identical* to the classical result. When more than one impact parameter contributes at a given scattering angle, $\sigma(\chi)$ is oscillatory. For rainbow scattering, which we discussed earlier, a schematic diagram of the differential cross section is shown in Fig. 6 indicating the difference between the wave-mechanical and classical behavior. That is, at large τ (close collisions) one impact parameter contributes and the semiclassical cross section follows the classical calculation. At small τ interferences occur and the semiclassical cross section oscillates about the classical result.

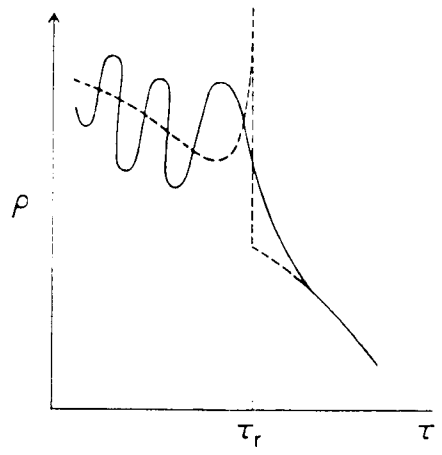

FIG. 6. Schematic diagram of angular differential cross section shown as ρ versus τ plot. τ_r indicates rainbow value for $E\chi_r$. Dashed curved, classical cross section; oscillation occurs where more than one trajectory contributes. [From R. E. Johnson (1982). "Introduction to Atomic and Molecular Collisions," p. 88. Plenum Press, New York.]

C. Other Approximations

Using the semiclassical expression for $\eta(b)$ given above and the impulse approximation, a simple estimate of $\eta^{sc}(b)$ that is applicable when (V/E) is small, is given in Table II. Using this in Eq. (25) *and* an approximation to $P_l(\cos\chi)$ valid at small angles, one obtains an estimate of $f(\chi)$ valid at small angles,

$$f(\chi) \simeq -\frac{m}{2\pi\hbar^2}\int d^3R\; V(R)e^{-i\,\Delta\mathbf{p}\cdot\mathbf{R}/\hbar} \tag{30}$$

This is referred to as the first Born approximation, and results for $\sigma(\chi)$ using Eq. (30) are given in Table II.

As $\eta(b) \xrightarrow{b\to 0} 0$ (see Table II) for potentials that decrease faster than $1/R$, the impulse approximation to $\eta(b)$ can be used to estimate the integrated cross section σ. That is, we replace $\sin^2\eta(b)$ by $\frac{1}{2}$ in Eq. (26) out to some large impact parameter $\bar{b}$ beyond which $\eta(b)$ is always small. Then $\sin^2\eta(b) \simeq \eta^2(b)$ at larger b, and σ is written

$$\sigma \simeq 2\pi\bar{b}^2 + 8\pi\int_{\bar{b}}^{\infty}\eta^2(b)b\, db \tag{31}$$

This is referred to as the Massey–Mohr approximation, and the result for power-law potentials is given in Table II. The expression given is finite for $n > 2$, unlike the classical result, which is never finite for a potential of infinite range. The cross section is also seen to decrease monotonically with increasing energy as shown earlier in Fig. (2). Using the optical theorem [Eq. (27)] in reverse, we see that, if σ is finite, then the

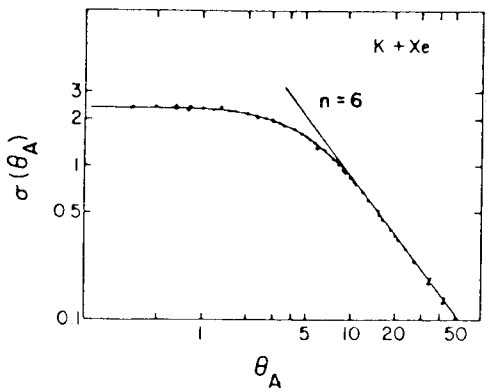

FIG. 7. Elastic scattering cross section (arbitrary units) versus laboratory scattering angle. Line indicates classical calculation using vander Waals potential. [Data from Helbing and H. Pauly (1964). *Z. Physik* **179**, 16. Figure from R. E. Johnson (1982). "Introduction to Atomic and Molecular Collisions," p. 163. Plenum Press, New York.]

differential cross section must be finite as $\chi \to 0$ (see Fig. 7), unlike the classical result. By contrast, a similar calculation of the diffusion cross section σ_d (or S_n) gives the *same form* as the classical expression [Eq. (13)] at small wavelengths. This comes about because scattering at $\chi = 0$ is excluded in the expression for σ_d. Therefore, classical expressions of the diffusion cross, and hence the nuclear stopping cross section, are accurate over a broad range of incident ion energies, allowing extensive use of classical estimates for ion penetration of gases and solids.

In the opposite extreme, when the wavelength is *large* compared to the dimensions of the scattering center ($K^{-1} \gg d$), then no classical analogies exist. However, only the lowest l values contribute in Eq. (25); hence, only one term is kept in the sum, so that

$$f(\chi) \approx \frac{1}{K} \sin \eta_0 \exp(i\eta_0) \qquad \text{and}$$

$$\sigma(\chi) = \frac{\sin^2 \eta_0}{K^2} \qquad (32)$$

(Note that if $\eta_0 \approx n\pi$ then higher terms are needed: this is referred to as the Ramsauer–Townsend effect.) The expression for the cross section in Eq. (32) represents the *same region of impact parameter* as the semiclassical result. However, at very low velocities, it is seen from Eq. (24) that an increase of l from 0 to 1 can make b very large. When b is much greater than the size of the colliding particles, d, then all interactions are encompassed, which at low velocities may only require a single value of l. In this limit it is seen that the differential cross section is *independent of angle for any potential*, a result obtained classically only for the collision of spheres. Because of its simplicity, an isotropic scattering cross section is often used in low-energy collisions, even when the large-wavelength criterion does not rigorously apply. At large wavelengths, the integrated cross section in Eq. (26) is simply written as

$$\sigma \approx \frac{4\pi}{K^2} \sin^2 \eta_0$$

which is also equal to the diffusion cross section σ_d at low velocities.

In the above we have considered very general properties of cross sections. In wave mechanics, as in the scattering of light, the cross sections will exhibit oscillatory behavior and/or resonances for a variety of potential forms. For example, when the long-range potential is attractive, a forward glory is seen in the integrated cross section. In the following sections we will briefly review the nature of interaction potentials, but in doing so we will also consider inelastic effects such as excitations and ionizations.

V. Interaction Potentials

A. Overview

The primary force determining the behavior of colliding atoms or molecules is the Coulomb interaction. This force acts between each of the constituent electrons and nuclei. Using Coulomb potentials the complete interaction potential for all of the particles can be immediately written down. However, each of the constituents moves relative to the center of mass of its parent molecule. As this motion is superimposed on the overall collisional motion, the description of a collision can be quite complex even for the simplest atoms. Rather than solve the wave equation for the complete, many-body system, one introduces the concept of single-interaction potentials averaged over the relative motion of the constituent particles. In using this concept we again exploit the huge mass difference between electrons and nuclei. This mass difference allows us, with reasonable accuracy, to separate the motion of the electrons and nuclei, a procedure referred to as the Born–Oppenheimer separation.

The behavior of the electrons during a collision is clearly going to depend on the relative motion of the nuclei. Therefore, interaction potentials are generally calculated in two limits. If the collisions are fast relative to the internal motion of the electrons ($v \gg v_e$), then during the collision the electronic distribution is static, except for abrupt changes (transitions) that occur when the particles are at their closest approach. The transitions reflect the ability of the molecules to absorb (emit) energy when exposed to the time-varying field of the passing particle in the same way that these molecules absorb or emit photons. Before and after the transition the potentials are determined from the separated charge distributions.

In the opposite extreme (slow collisions, $v \ll \bar{v}_e$) the electrons adjust continuously and smoothly to the nuclear motion, returning to their initial state at the end of the collision. This collision process is called adiabatic as the electrons do not gain or lose energy. That is, even though the molecules may be deflected and change kinetic energy, their initial and final *elec-*

tronic states remain the same. The electronic distribution evolves from a distribution in which electrons are attached to separate centers at large R to a distribution in which the electrons are shared by the two centers at small R, a covalent distribution. Therefore, for every possible initial state there is a corresponding adiabatic potential, resulting in rather complex potential diagrams. Such potentials also determine the ability of the two particles to bind together to form a molecule.

As molecules in a collision are not moving infinitely slowly, the motion of the nuclei can induce transitions between states. For near-adiabatic collisions these transitions occur at well-defined internuclear separations—for example, at those internuclear separations at which the atomic character of the wave function gives way to the molecular, covalent character. Because a large computational effort is required to obtain the set of potential curves, and an additional large computational effort is required to describe the collisions when transitions occur, simplifying procedures are very attractive and approximate potentials are often constructed.

As the electrons in different shells have very different velocities, the above separation into fast and slow collisions allows us to treat the orbitals separately. For instance, when a collision is fast with respect to the outer-shell electrons, it may be adiabatic with respect to the inner-shell electrons. Therefore, the inner-shell electrons return to their initial state. Their effect is to only screen the nuclear interactions and, hence, they play a passive role in the collision. Alternatively, when inner-shell excitations occur the outer-shell electrons can be considered to be static during the collision. As a point of reference, it is useful to remember that a nucleus with a speed equivalent to an electron in the ground state of a hydrogen atom has an energy of about 25 keV/amu. Further, the orbital speed of an electron in an atom can be scaled to the speed of an electron in the ground state of hydrogen using the effective nuclear charge.

The interaction potential between two atoms can be written as a sum of the nuclear repulsion and the averaged electronic energy $\varepsilon_j(R)$,

$$V_j(R) = \frac{Z_A Z_B e^2}{R} + [\varepsilon_j(R) - \varepsilon_j] \qquad (33)$$

In this expression j labels the electronic state, Z_A and Z_B are the nuclear charges, and ε_j is the total electronic energy of the colliding atoms, $\varepsilon_j(R)$, as $R \to \infty$. Each state j is associated with a pair of separated atomic states at large R. In the *electrostatic limit* ($v \gg \bar{v}_e$), the electronic energy $\varepsilon_j(R)$ is a sum of the electronic energies of the separated atoms, $(\varepsilon_{Aj} + \varepsilon_{Bj}) = \varepsilon_j$, *plus* the averaged interaction of the electrons on each atom with the electrons and nucleus of the other atom, which we call V_j^e. The quantity V_j^e is written

$$V_j^e(R) = -Z_B e^2 \int \frac{\rho_{Aj}(\mathbf{r}_A)}{|\mathbf{R} - \mathbf{r}_A|} d^3 r_A - Z_A e^2 \int \frac{\rho_{Bj}(\mathbf{r}_B)}{|\mathbf{R} - \mathbf{r}_B|} d^3 r_B + e^2 \int \frac{\rho_{Aj}(\mathbf{r}_A)\ \rho_{Bj}(\mathbf{r}_B)}{|\mathbf{R} - \mathbf{r}_A + \mathbf{r}_B|} d^3 r_A\, d^3 r_B \qquad (34)$$

where the ρ_{Aj} and ρ_{Bj} are the atomic densities for the electrons on atoms A and B. V_j^e is the classical electrostatic interaction and is evaluated in many texts for various form for ρ.

In the adiabatic approximation, $\varepsilon_j(R)$ in Eq. (33) is calculated from the full electronic wave equation at each R. An approximation that is particularly useful for light atoms is to estimate $\varepsilon_j(R)$ via the molecular-orbital method used by chemists. For heavy atoms, on the other hand, the Thomas–Fermi method is often employed to estimate $\varepsilon_j(R)$. In this model the electrons are treated as a gas subject to the Pauli principle. In the following, rather than calculate, $V_j(R)$ for all R, we will consider its behavior for various regions of R. Such an approach is reasonable as it is seen from Table II that the deflection function is determined primarily by a narrow region of R about the distance of closest approach.

B. Short-Range Potentials

For close collisions ($R \ll \bar{r}_A, \bar{r}_B$ where $\bar{r}_A$ and $\bar{r}_B$ are the mean atomic radii), the nuclear repulsion dominates. The electrons essentially screen the nuclear repulsive interaction; hence, one often approximates $V_j(R)$ by

$$V_j(R) = \frac{Z_A Z_B e^2}{R} \Phi\left(\frac{R}{a_j}\right) \qquad (35)$$

where a_j is a screening length and Φ the screening function. Considerable effort has been expended determining Φ and a_j for many-electron atoms and often Φ is written as $\exp(-R/a_j)$. At small distances of closest approach which are usually associated with fast collision, an electrostatic calculation [Eq. (34)] can be used to esti-

mate Φ and a_j. In fact, the electrons in different shells have different screening lengths. Therefore, for a bare ion colliding with an atom, a potential of the form

$$V_j(R) = \frac{Z_A e^2}{R} \sum_i N_{B_i} e^{-R/a_i}$$

is used, where N_{B_i} is the number of electrons in the ith shell on B. A good approximation for light atoms is to assume that the ith shell has a screening constant determined by the ionization energy I_i, $a_i \approx a_0/Z_i'$ with the effective charge $Z_i' = (I_i/I_0)^{1/2}$, where I_0 is the ground-state, hydrogen atom ionization potential.

For collisions between large atoms ($Z \gtrsim 10$), the Thomas–Fermi screening constant used by Lindhard,

$$a_{TF} = 0.8853 a_0 \, (Z_A^{2/3} + Z_B^{2/3})^{-1/2} \qquad (36)$$

has been shown to be generally applicable and more elaborate functional forms for Φ are employed. Expressions for cross section and stopping cross section have been given in Table II for the potential in Eq. (35) using the exponential screening function. Results obtained by Lindhard for the Thomas–Fermi screening function are also given. As the short-range collision region has been extensively studied, one should be careful to use experimentally determined parameters when available.

C. Long-Range Interactions

For slow collisions even small disturbances can lead to deflections; therefore the interaction potential at long range (large separations between colliding partners, $R >> \bar{r}_A, \bar{r}_B$) is of interest. As the electronic distributions of each of the colliding particles are distorted very little by the presence of the other, the interaction potential is written in powers of R,

$$V_j(R) = \sum C_n / R^n \qquad (37)$$

and, generally, only the largest term (lowest power of n) is kept in a calculation. Therefore, the power-law expression for cross section that we developed earlier can be used for weak-interaction, long-range collisions. The lead terms in Eq. (37) can be obtained from the electrostatic interaction in Eq. (34) by expanding the denominators in powers of R. For ion–ion collisions the lead term in Eq. (37) is $n = 1$, $C_1 = \bar{Z}_A \bar{Z}_B e^2$, which is the coulomb interaction with $\bar{Z}_A = Z_A - N_A$ (the nuclear charge of A minus the number of electrons on A or the net charge). For ion collisions with a neutral molecule having an electric dipole moment μ_B (e.g., water molecule), the lead term is $n = 2$, $C_2 = \bar{Z}_A \mu_B e \cos\theta$ where $\cos\theta$ is the angle between the internuclear axis and the dipole moment. For neutral molecules that do not have dipole moments (e.g., O_2, N_2), the ion–quadrupole interaction dominates ($n = 3$). For two neutral molecules having dipole moments, the dipole–dipole interaction ($n = 3$) dominates, and so on.

For colliding atomic particles the electrostatic multipole moments of the charge distribution are zero and for some molecules (e.g., H_2) the multipole moments are small. However, the field of the other particle induces moments in the separated charge distribution. The lead term for ion-neutrals is the ion-induced dipole interaction ($n = 4$),

$$C_4 = -\frac{\alpha_B}{2} (\bar{Z}_A e)^2$$

where α_B is the polarizability of the neutral particle B. For collisions between two neutrals there is not average field at B due to A or vice versa. However, instantaneous fluctuations in charge density on either atom lead to short-lived fields that induce moments in the other. Therefore, for neutrals the lead term is the induced-dipole–induced-dipole interaction, which is the well-known van der Waals potential used to describe the behavior of realistic gases. This interaction ($n = 6$) is always attractive (i.e., C_6 negative) and the coefficients have been extensively evaluated from collision experiments.

D. Intermediate Range Potentials and Charge Exchange

When R is the order of the atomic radii ($\bar{r}_A$, $\bar{r}_B$), the electron clouds on the two interacting particles overlap. In this region the distortion of the charge clouds on each center becomes too large to treat as simply a perturbative polarization of the separated electronic distributions. This is an especially important region for determining transitions between colliding particles but is also important in molecular structure determinations. The emphasis here is on those aspects important in collisions.

The overlap of charge on the two centers allows for the possibility of charge-exchange collisions (e.g., $H^+ + O_2 \rightarrow H + O_2^+$). When charge exchange occurs the potentials before and after the collisions can be drastically different. For

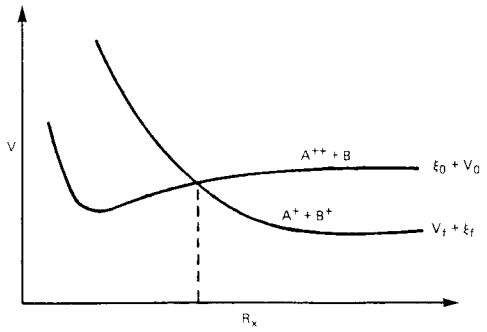

FIG. 8. Interaction potentials versus internuclear separations; curve crossing for the $A^{2+} + B \rightarrow A^{+} + B^{+}$ collisions.

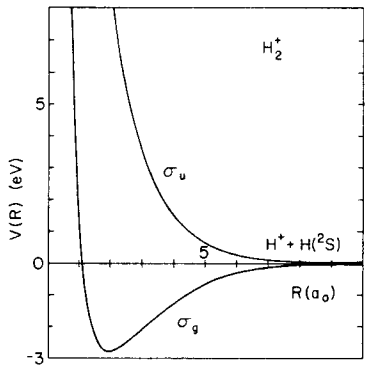

FIG. 9. Interaction potential energy curves versus internuclear separation for ground state H_2^+: nuclear repulsive plus electronic (ε_g or ε_u).

example, for $O^{2+} + S \rightarrow O^{+} + S^{+}$, a process of interest in the Jovian magnetosphere plasma, the initial long-range interaction is attractive and is determined by the polarizability of S. On the other hand, the final interaction is clearly repulsive. Depending on the final states of O^+ and S^+, the initial and final potential curves may cross as shown in Fig. 8. Therefore, electron exchange between O^{2+} and S can occur with *no net change* in the total electronic energy *at* the crossing point. Of course, the change in state gradually results in a net change in the *final* electronic energy as the particles separate. Therefore, such crossings indicate transition regions and the likelihood of charge exchange is determined by the overlap of the charge distributions at the crossing point.

For this region of intermediate R the covalent (electron exchange) interaction can be examined by considering the $H^+ + H$ (i.e., H_2^+) system. In such a system, the exchange $H^+ + H \rightarrow H + H^+$ occurs *without* a net change in internal energy, unlike the case discussed above. The two identical states at large R ($H + H^+$ and $H^+ + H$) split at smaller R, due to electron sharing, forming both attractive and repulsive potentials, as shown in Fig. 9. If the wave functions placing the electron on centers A and B in identical states of the hydrogen atom are ϕ_A and ϕ_B, then the linear combination appropriate to the H_2^+ molecule are $\psi_{g,u} \cong (1/\sqrt{2})(\phi_A \pm \phi_B)$. The labels g and u refer to symmetric and antisymmetric (gerade and ungerade) states of H_2^+. In the scattering of protons by hydrogen, as the initial state is *either* ϕ_A *or* ϕ_B, half the collisions will be along repulsive potentials (u state) and half along an attractive potential (g state). The difference in energy between these states is referred to as the exchange energy and will determine the behavior of charge-exchange collisions. This exchange energy decays as the overlap of the wave functions on A and B ($<\phi_A|\phi_B> \alpha e^{-R/\bar{a}}$), which is an exponential function. Therefore, this exchange interaction is eventually dominated at very large R by the long-range, power-law potentials discussed earlier.

Molecular orbital potentials for H_2^+ can also be constructed for each excited state of H, or, more usefully, they can be constructed for one electron in the field to two identical nuclei *and* other electrons. In Fig. 10 we give a diagram showing the general behavior of these one-elec-

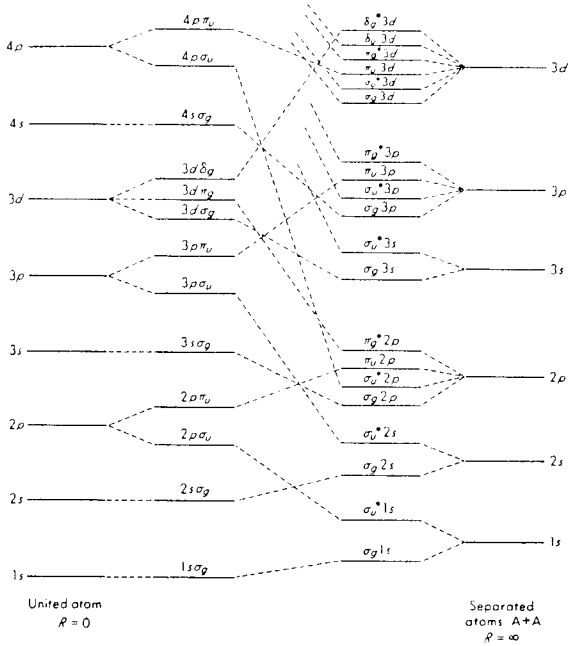

FIG. 10. Correlation diagram for one electron on two identical centers with effective charge Z'_A. [From R. E. Johnson (1982). "Introduction to Atomic and Molecular Collisions," p. 124. Plenum, New York.]

tron, molecular orbital binding energies $\varepsilon_j(R)$. As this quantity does not include the nuclear repulsive term in Eq. (33), we can follow the behavior of these states down to $R = 0$. This diagram correlates the one-electron states of the separated centers ($R \to \infty$) with those of the united atom ($R \to 0$), indicating how the electronic binding energy changes versus R. The states are labeled by their symmetry (g or u) under inversion and by the component of electronic angular momentum along the internuclear axis ($|m_l| = 0,1,2,\ldots$ as $\sigma,\pi,\delta,\ldots$). The correlation between states at large and small R is determined by the fact that states of the same symmetry [rotation $|m_l|$ and inversion (g, u)] do not cross (i.e., do not become degenerate in energy). Two sets of notation are used for these states in order to indicate which are the corresponding atomic states at either $R \to 0$ or $R \to \infty$. For example, the two lowest states we considered above for H_2^+ are labeled $\sigma_g 1s$ and $\sigma_u 1s$ at large R, indicating they originate from the ground state (e.g., 1s state of H). At small R they are labeled $1s\sigma_g$ and $2p\sigma_u$, indicating they correlate with the 1s and 2p states of the united atom (e.g., He^+ for the H_2^+ molecule).

To obtain interaction potentials for a particular pair of atoms the net binding energy of each electron, determined from the correlation diagram and the Pauli principle, is combined with the nuclear repulsive potential in Eq. (33). Therefore, two hydrogen atoms (H_2) interact via a singlet state $(\sigma_g 1s)^2\ {}^1\Sigma_g^+$ which is *attractive* at intermediate R, and a triplet state $(\sigma_g 1s)(\sigma_u 1s)\ {}^3\Sigma_u^+$. The latter is a net *repulsive* potential at intermediate and small R (i.e., ignoring the polarization at very large R). Therefore, for the collision between two H atoms $\frac{3}{4}$ of the collisions are repulsive and $\frac{1}{4}$ attractive. Two helium atoms (He_2) interact via a $(\sigma_g 1s)^2\ {}^1\Sigma_g^+$ ground repulsive state. The lowest state for two oxygen atoms is $(\sigma_g 1s)^2\ (\sigma_g 1s)^2\ (\sigma_g 2p)^2\ (\pi_u 2p)^4\ (\pi_g 2p)^4\ (\sigma_g 2s)^2\ {}^3\Sigma_g^+$. In the above the $\Sigma,\Pi,\Delta,\ldots$ represent the *net* angular momentum along the internuclear axis ($|\Sigma m_{li}| = 0,1,2,\ldots$, where i implies a sum over orbitals). These states are all doubly degenerate (i.e., the angular momentum vector can be pointed either way) except the Σ states, which are, therefore, also labeled according to their behavior under reflection (+ or −) about a plane containing the nuclei. [*See* POTENTIAL ENERGY SURFACES.]

The molecular orbital diagrams are extremely useful for determining which transitions are likely to occur. Following the molecular orbital states at large R into small R will result in a number of curve crossings as seen in the potential diagram for certain states of He_2^{2+} in Fig. 11. In a full adiabatic calculation of the electronic energies, for which the electrons *totally* adjust to one another, crossings are avoided for states of the same total symmetry. Therefore the crossings in the molecular orbital diagram indicate that value of R at which the character of the wave function is changing and hence indicate the transition regions. The $(\sigma_u 1s)^2\ {}^1\Sigma_g^+$ state of He_2^{2+} is seen to make a series of crossings as both of the electrons are promoted to (2p) electrons in the united atom limit. Therefore, half of the collisions for He^{2+} on He will proceed along an attractive ${}^1\Sigma_u^+$ for which transitions *are unlikely* at low velocities and half along a strongly repulsive ${}^1\Sigma_g^+$ state for which transitions are *very likely* to occur if the distance of closest approach is small enough. As pointed out by Lichten and Fano, such electron promotion occurs in all colliding systems as there are two atomic orbital states at large R for every atomic orbital state at small R (see Figs. 9 and 10).

A molecular orbital correlation diagram can also be constructed for an electron in the field of two positive centers having different effective charges Z_A and Z_B. As the inversion symmetry is broken, the correlations are determined using $|m_l|$ only, thereby lessening the promotion effect. The importance of promotion, and hence transition, depends in part, therefore, on how similar the effective charges are on each center. For instance, for a proton interacting with an argon atom (ArH^+ potential), the ground-state potentials at intermediate R are well described by a single electron shared by an Ar^+ core and a proton. As these have binding energies $I_{Ar} = 15.2$ eV and $I_H = 13.6$ eV, the effective charges are very similar ($Z'_{Ar} = 1.06$, $Z'_H = 1$). Therefore, the lowest Σ states of ArH^+ are similar to those of H_2^+ at intermediate R. Stated another way, states of the same symmetry that are close in energy at large R are strongly coupled; therefore, they tend to "repel" (diverge) from each other. The covalent nature of these states is associated with an exchange interaction similar to that in H_2^+, which we write in a general form as

$$\Delta\varepsilon = A \exp(-R/\bar{a}) \tag{38}$$

where the effective radius is $\bar{a} = 2a_0/(Z'_A + Z'_B)$.

This confusion of potentials presents problems for the user. For example, although the $O^+ + O$ (O_2^+ system) has a lowest-lying attractive (bound) state ${}^2\Pi_g$, in a collision of a ground-state oxygen ion with a ground-state oxygen atom seven different potential curves evolve,

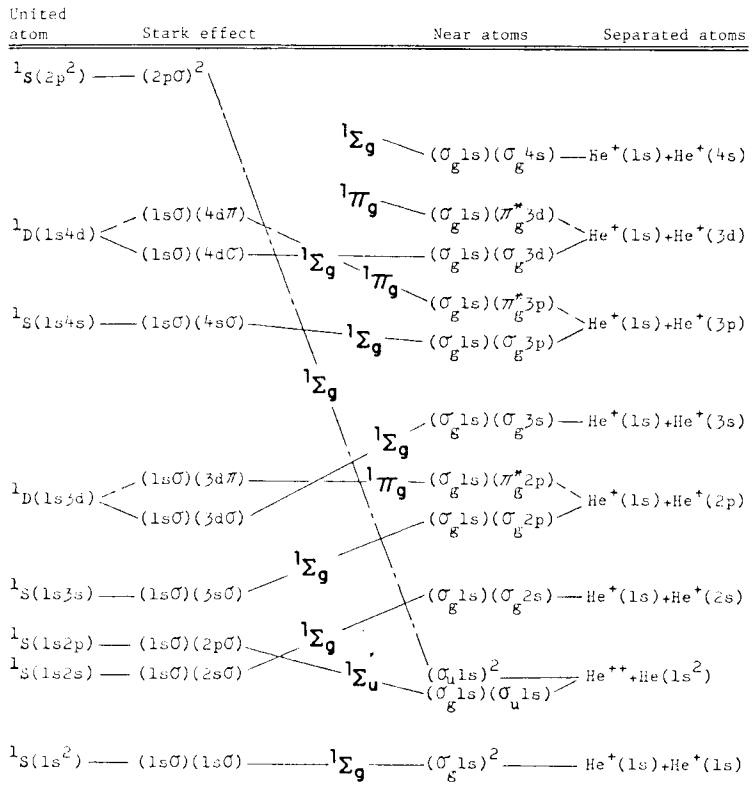

FIG. 11. Correlation diagram for certain states of He_2^{2+}. He^{2+} + He gives a $^1\Sigma_g$ that crosses many states and a $^1\Sigma_u$ that does not. [From R. E. Johnson (1982). "Introduction to Atomic and Molecular Collisions," p. 123. Plenum, New York.]

each with a different multiplicity. Therefore, simplifying procedures are desirable. Although it is not strictly correct to use a single potential, the repulsive curves often dominate and a simple repulsive potential is often used to approximate the interaction at intermediate R. Based on the form for electron exchange interaction discussed above, this potential is generally represented as an exponential, $V = Ae^{-R/a}$. Such a potential is called a Moliere potential and is commonly used in particle penetration calculations. It can be thought of as an extension of the short-range, repulsive interactions discussed earlier. In fact, a universal potential form intended to cover both ranges of R for heavy elements is the Lenz–Jensen form for Φ in Eq. (35), which we give in Table II.

VI. Inelastic Collisions

A. Overview

The calculation of the changes in internal motion of a molecular system of particles induced by a collision with another atom or molecule is a complicated many-body problem for which a number of approximate models have been developed. When the interacting particles are moving, as in a collision, then the interactions described in the preceding sections become dynamic. In addition to the overall deflections, calculated by the potentials described, the time-dependent fields produce changes in the internal state of the molecule. The motion of each of the constituent particles of the molecules can be characterized by a frequency ω and a mean radial extent from the center of mass, $\bar{r}$. The interaction with a passing particle of velocity v at a distance b from the center of a target atom or molecule is said to be nearly adiabatic if $\tau_c \gg \omega^{-1}$ where $\tau_c \approx b/v$. For nonadiabatic collisions, transitions become likely, as discussed in Section I,B.

In most instances, the approximations used involve only two states. Such models can be divided into two categories: strong interactions, for which the evolution of the electronic states during the collision is important (e.g., curve-crossing transitions) and weak interactions, for which the initial charge distributions can be considered static. The former case generally applies

to incident ion velocities comparable to or smaller than the velocities of the constituent particles of the target and the latter to large velocities. If, in addition, $b \ll \bar{r}$, then the collision is a close collision and the incident particle can be thought of as interacting with each of the constituents of the target molecule separately. This is referred to as the binary-encounter limit. On the other hand, if $b \gg \bar{r}$, a distant collision, the target atom or molecule must be viewed as a whole. Classically the constituent particles are often treated as bound oscillators of frequency ω. These oscillators are then excited by the time-dependent field of the passing particle. (Of course, in wave mechanics the impact parameter is not a well-defined concept and the close and distant criterion is based, more correctly, on whether the momentum transfer to the constituent particles is large or small.) In the following we calculate, classically, the large-momentum transfer (close collision) and small-momentum transfer (distant collision) contributions to the energy-loss cross section. These results are synthesized by considering the Bethe–Born approximation to the cross section. Following this we consider models for strong interactions such as charge exchange.

B. Binary-Encounter Approximation

In the often-used binary-encounter approximation (BEA), each target constituent is assumed to interact separately with the incident particle. For example, the stopping power [Eq. (11)] can be written as a sum of contributions from each of the constituents:

$$S = S_e + S_n \approx \sum_j N_j \int Q \, d\bar{\sigma}_j(Q) + \sum_k \int T \, d\sigma_k(T) \tag{39}$$

The differential cross section $d\bar{\sigma}_j(Q)$ is the energy-transfer cross sections to the electrons in orbit j with population N_j and $d\sigma_k(T)$ is the energy-transfer cross section to nucleus k in the target molecule. The latter contribution we considered earlier when describing elastic collisions. Results are given in Table II for $d\sigma(T)$ $[\equiv (d\sigma/dT)\, dT]$ and S_n for a single nucleus using a number of potentials. We note in passing that the total S_n can be rewritten for a molecular target having more than one nucleus in such a way that the energy transfer to the center of mass of the target molecule and that energy going into vibrational and rotational excitation of the molecule are separated. The latter contributions are, in fact, inelastic effects and, of course, sufficient collisional energy transfer can lead to dissociation of a molecular target. If M is the total molecular mass and D_k the removal energy for nucleus k of mass M_k, then the BEA estimate for the collisional dissociation cross section is

$$\sigma_D \approx \sum_k \int_{MD_k/(M-M_k)}^{\gamma_{Ak}E_A} d\sigma_k(T) \tag{40}$$

This is easily calculated using the results in Table II.

The cross section $d\bar{\sigma}_j(Q)$ in the BEA is an "elastic" cross section for a collision between the incident particle and a free electron leading to a change Q in the electron's energy. The bar implies an averaging over the initial orbital velocity distribution of the electron. In general, any appropriate cross section can be used to describe the target electron–incident particle collision. If the incident particle is a bare ion of charge Z_A, then the collision with the electrons is coulombic. If, further, the ion's velocity is large compared to the mean orbital velocity of the electrons, then the averaging is not important and collision is described by the Rutherford cross section

$$d\bar{\sigma}_j(Q) \approx \frac{2\pi}{m_e v^2}\left(\frac{Z_A e^2}{Q}\right)^2 dQ \tag{41a}$$

(e.g., use results in Table II with $M_B \to m_e$, $n = 1$, $c_1 = Z_A e^2$, and $T \to Q$). Using this cross section in Eq. (39), the reader can verify that electronic stopping cross section [e.g., Eq. (12a)] can be written

$$S_e \approx \frac{2\pi}{m_e v^2}(Z_A e^2)^2 \sum_j N_j \ln \frac{2m_e v^2}{(Q_j)_{\min}} \tag{41b}$$

where $(Q_j)_{\min}$ and $2m_e v^2$ are the lower and upper limits on the energy transfer to the "stationary" electrons. Similarly, the BEA approximation to the total ionization cross section for fast ions, referred to as the Thompson cross section, is

$$\sigma_I \approx \frac{2\pi}{m_e v^2}(Z_A e^2)^2 \sum_j N_j \left(\frac{1}{I_j} - \frac{1}{2m_e v^2}\right) \tag{41c}$$

where I_j is the removal energy for electrons in the jth orbit. The BEA ionization and stopping cross sections for incident ions vary as $1/E_A$ and $(\ln E_A)/E_A$ respectively at high energies. For an incident neutral a screened Coulomb cross section should be used for $d\bar{\sigma}_j(Q)$; for example, the Born approximation for the screened Coulomb interaction is given in Table II with $M_B \to m_e$ and $T \to Q$. Using these the *form* for S_e and σ_I

will closely resemble that of S_n and σ_D calculated using a screened Coulomb potential.

C. Classical Oscillator

For distant-collisions, and low-momentum transfer collisions, we can treat the bound electrons and/or nuclei as classical oscillators that are excited by the time-varying field of the passing particle. The motion of an electron oscillator in a field $\mathscr{E}_j(t)$ is

$$m_e\ddot{\mathbf{r}}_j + \Gamma_j\dot{\mathbf{r}}_j + m_e\omega_j^2\mathbf{r}_j = -e\mathscr{E}_j(t) \qquad (42)$$

where ω_j is the binding frequency and Γ_j is a damping constant. Writing the energy transfer as

$$Q_j = \int_{-\infty}^{\infty} \dot{\mathbf{r}}_j\cdot[-e\mathscr{E}_j(t)]\,dt$$

then as $\Gamma_j \to 0$ it is straightforward to show that

$$Q_j \to \frac{\pi}{m_e}|e\mathscr{E}_j(\omega)|^2$$

where $\mathscr{E}_j(\omega)$ is the Fourier transform of $\mathscr{E}_j(t)$, that is,

$$\mathscr{E}_j(\omega) = \frac{1}{\sqrt{2\pi_i}}\int_{-\infty}^{\infty}\mathscr{E}_j(t)\,\exp(-i\omega t)\,dt$$

Note that $|e\mathscr{E}_j(\omega)|$ has units of momentum, indicating the net impulse to the oscillator.

Describing $\mathscr{E}_j$ as the field associated with a screened coulomb potential, $V = (Z_Ae^2/R)e^{-\beta R}$ and assuming straight line trajectories ($R^2 = b^2 + v^2t^2$), the energy transfer is

$$Q_j = \frac{2(Z_Ae^2)^2}{m_ev^2}\left(\frac{1}{b^2}\right)\left[(\beta_j'b)^2K_1^2(\beta_j'b) + \left(\frac{\omega_jb}{v}\right)^2K_0^2(\beta_j'b)\right] \qquad (43a)$$

where $\beta'^2 = \beta^2 + (\omega_j/v)^2$ and K_1 and K_0 are modified Bessel functions. This energy transfer behaves asymptotically as

$$Q_j \to \frac{2(Z_Ae^2)^2}{m_ev^2}\left(\frac{1}{b^2}\right)\begin{cases}\left.\begin{array}{ll}1 & \text{for}\quad b\beta \ll 1\\ \frac{\pi}{2}(\beta b)\exp(-2\beta b) & \text{for}\quad b\beta \gg 1\end{array}\right\}\frac{\omega_jb}{v} \ll 1\\ \frac{\pi}{2}\left(\frac{\omega_jb}{v}\right)\exp\left(\frac{-2\omega_jb}{v}\right);\quad \frac{\omega_jb}{v} \gg 1,\ \frac{\omega_j}{v} \gg \beta\end{cases} \qquad (43b)$$

It is important to note in these expressions that screening of the collision is a result *both* of the direct screening in the potential via β [$\beta \to a_j^{-1}$ in Eq. (35)] and that due to the motion of the electron via ω_j. In Eq. (43b), $(\omega_jb/v \ll 1)$ is the classical BEA limit for a screened coulomb potential, in which the incident ion is fast compared to the bound electron motion; Q decreases rapidly for $b > \beta^{-1}$. Further, $(\omega_jb/v \gg 1)$ is the adiabatic limit as described earlier; Q is seen to decrease rapidly for $b > v/\omega_j$. Writing the electronic stopping power as

$$S_e = \sum_j N_j 2\pi\int_{(b_{min})_j}^{\infty} Q_j(b)b\,db$$

where N_j is the number of electrons of frequency ω_j and using Eq. (43a) the expression for S_e is exactly integrable. Setting b_{min} equal to the wavelength in the center of mass of the electron–incident–ion system ($\hbar/m_ev$), then

$$S_e \simeq 4\pi\frac{(Z_Ae^2)^2}{m_ev^2}\sum N_j\left[\ln\left(\frac{1.123m_ev}{\beta_j'\hbar}\right) - \frac{1}{2}\left(\frac{\beta}{\beta_j'}\right)^2\right] \qquad (44a)$$

When the direct screening dominates (i.e., $\beta_j' = \beta$ for large v), then Eq. (44a) has the form of Eq. (41b) with $Q_{min} \propto \beta^2\hbar^2/(2m_e)$. That is, the screening constant β determines the low energy cutoff. On the other hand, when $\beta = 0$ (i.e., no direct screening), then

$$S_e \simeq 4\pi\frac{(Z_Ae^2)^2}{m_ev^2}\sum N_j\left(\ln\frac{1.123m_ev^2}{\hbar\omega_j}\right) \qquad (44b)$$

This is roughly twice the BEA result given in Eq. (41b). The origin of this factor of two will be clear from the subsequent discussion. Here we only point out that this classical oscillator model very nicely describes both distant and close collisions when calculating the energy loss cross section. However, it is much less useful for determining, for instance, the ionization cross section.

D. Bethe–Born

The first-order estimate of the inelastic cross section in quantum mechanics is given by the Born approximation. The Born scattering amplitude for a transition from an initial state (0) to a final state (f) is given by

$$f_{0\to f} \approx \frac{-m}{2\pi\hbar^2}\int e^{-i\mathbf{K}_f\cdot\mathbf{R}}V_{f0}(R)e^{i\mathbf{K}_0\cdot\mathbf{R}}\,d^3R \qquad (45a)$$

This leads to a cross section, as in Eq. (23), of

the form

$$\sigma_{0\to f}(\chi) = \frac{K_f}{K_0}|f_{0\to f}|^2 \qquad (45b)$$

where $\hbar K_f$ and $\hbar K_0$ are the final and initial momentum and $\cos\chi = \hat{K}_f \cdot \hat{K}_0$. In Eq. (45a) the exponentials represent incoming and outgoing plane waves and $V_{f0}(R)$ is the interaction potential averaged over the final and initial states. Equation (45) can be related to Eq. (30), the elastic scattering result. For elastic scattering, the final and initial electronic states are identical; therefore $\mathbf{K}_j$ and $\mathbf{K}_0$ are the same size but differ only in direction. In describing elastic scattering, the potential $V_{00}(R)$ is simply the electrostatic potential for the ground state that we called $V_0(R)$ in Eq. (33). In addition, $e^{i(\mathbf{K}_0-\mathbf{K}_f)\cdot\mathbf{R}} = e^{-i\Delta\mathbf{p}\cdot\mathbf{R}/\hbar}$, yielding the result in Eq. (30).

For a fast collision of an incident ion with a neutral, Bethe approximated the cross section above as

$$d\sigma_{0\to f} \simeq \frac{2\pi(Z_A e^2)^2}{m_e v^2} Z_B \frac{dQ}{Q^2}|F_{0\to f}(Q)|^2 \qquad (46)$$

where $Q = \Delta\mathbf{p}^2/2m_e$ and the quantity $F_{0\to f}(Q)$ is the interaction matrix element of the target atom. Note that if $|F_{0\to f}|^2 = 1$, this expression becomes identical to the Rutherford cross section above. Equation (46) differs from the BEA in that $\Delta\mathbf{p}$ is *not* the momentum transfer to a single electron but to the system as a whole. Hence, even for very small net change in momentum, electronic transitions, which require significant internal energy changes, *can* occur. The interaction matrix element is a weighting factor, which has the property that

$$\sum_f (\varepsilon_f - \varepsilon_0)|F_{0\to f}(Q)|^2 = Q$$

so that the *average* effect of all the electronic transitions is an energy change equal to that used in the BEA. $F_{0\to f}(Q)$ contains the screening effect of the moving electron, so that for large-momentum transfers, and hence large Q,

$$|F_{0\to f}(Q)|^2 \approx \begin{cases} 0 & \varepsilon_f - \varepsilon_0 \neq Q \\ 1 & \varepsilon_f - \varepsilon_0 = Q \end{cases}$$

On substitution into Eq. (46) this gives the classical BEA result, Eq. (41a), discussed earlier. This means that for large energy transfers, the momentum transfer is, with a *high probability*, equal to that transferred to a single electron raising it to an excited state. At small momentum transfers, hence low Q,

$$Z_B|F_{0\to f}(Q)|^2 \approx \left(\frac{Q}{\varepsilon_f - \varepsilon_0}\right) f_{0f}$$

This is the limit in which the excitations are predominantly dipole excitations and f_{0f} is the dipole oscillator strength, which is also used to determine the polarizability of an atom in the field an ion. [*See* ATOMIC PHYSICS.]

Using these expressions for the generalized oscillator strength to calculate the stopping power, one finds the remarkable result that the *form* of the stopping power is the same at high and low Q (or Δp), so that the result is *not* sensitive to the value of Q dividing these regions. The combined stopping power can be written

$$S_e \equiv \sum_f \int (\varepsilon_f - \varepsilon_0)\, d\sigma_{0\to f}$$
$$\approx \frac{4\pi(Z_A e^2)^2}{m_e v^2} Z_B \left(\ln\frac{2m_e v^2}{I} - 1 - C\right) \qquad (47)$$

In this expression the sum over states is absorbed in the values of I and C. Here C is a factor associated with the shell structure of the target atom or molecule and I is an average ionization potential. Values of I and C have been extracted from experiment. This expression for S_e has the same form as that in Eq. (44b) for the coulomb interaction with an oscillator and, therefore, is also twice the BEA result at high velocities. The value of 2 indicates that the distant *and* close collisions described here contribute roughly equally to S_e.

The quantities above can also be used to determine the leading terms at large v for total ionization cross section σ_I and the straggling cross section $S_e^{(2)}$. The lead term at large v is

$$\sigma_I \equiv \sum d\sigma_{0\to f} \approx \frac{4\pi(Z_A e^2)^2}{m_e v^2}\left(\frac{2m_e\overline{r_0^2}}{3\hbar^2}\right)\ln\left(\frac{2mv_e^2}{I}\right) \qquad (48a)$$

where f implies all final states leading to an ionization and $\overline{r_0^2}$ is the mean-squared radius of the initial state. Similarly,

$$S_e^{(2)} \equiv \sum \int (\varepsilon_f - \varepsilon_0)^2\, d\sigma_{0\to f} \approx 4\pi(Z_A e^2)^2 Z_B \qquad (48b)$$

which is summed over all final states, ionizations, and excitations. The latter quantity, which weights large energy transfers heavily, is equal to the BEA calculation at high velocities as close collisions (large momentum transfers) dominate. On the other hand, the ionization cross section, which unlike S_e and $S_e^{(2)}$ is not weighted by the energy transfer, is determined

primarily by *dipole* excitations (small momentum transfers). The ionization cross, therefore, is *not* very well represented by Thompson expression in Eq. (41c); rather, it has a similar energy dependence, for fast incident ions, to that of the stopping cross section, i.e., $(\ln E_A)/E_A$. This commonality in energy dependence has the very useful consequence that the *number of ionizations* per unit path length produced by a fast incident ion stopping in a gas or solid is roughly proportional to S_e.

E. Two-State Models: Charge Exchange

For collision velocities comparable to or smaller than the speed of the constituents of the target particles, the details of the interaction potentials described earlier can control the transition probability. When the coupling between neighboring states is strong and the existence of other states can be treated as a weak perturbation, a number of two-state models can be used for calculating these probabilities. The models are based on the impact parameter cross section in Eq. (7), and forms for the transition probabilities $P_{0\to f}$ are given in Table III. A requirement for strong coupling is that the energy difference between the states at any point in the collision is small compared to the uncertainty in the energy of the states during the collision. This uncertainty is estimated as $\Delta E \approx \hbar(\Delta R_x/v)$ where ΔR_x is the extent of the transition region. The general nature of these two-state inelastic cross sections was described earlier. At low velocities (ΔE above much less than the state spacing, $\varepsilon_f - \varepsilon_0$), the levels are well defined and transitions are not likely. At high velocities the uncertainty ΔE becomes large so that the states effectively overlap. However, at high velocities, the time for a transition to occur becomes short so that transition probabilities again become small and the Born approximation described above should be used. When the spacing between states during the collision is comparable to ΔE, then the cross section is large (i.e., $\sim\pi a_0^2$ for transition involving outer-shell electrons).

TABLE III. Inelastic Collision Expressions

Impact parameter results

$$\left(\sigma_{0\to f} = 2\pi \int_0^\infty P_{0\to f}(b) b\, db,\ \varepsilon_f - \varepsilon_0 \equiv \hbar\omega_{f0} \equiv Q_{0\to f}\right)$$

First order (Born)

$$P_{0\to f}(b) \approx \left|\frac{1}{i\hbar}\int_{-\infty}^{\infty} \Delta\varepsilon_{0f}(R)\exp(i\omega_{f0}t)\, dt\right|^2$$

for $\Delta\varepsilon_{0f} = V_0 e^{-\beta R}$

$$P_{0\to f}(b) \approx \left(\frac{2V_0 b}{\hbar v}\right)^2 \left(\frac{\beta}{\beta'}\right)^2 K_1^2(b\beta')$$

$$\beta'^2 = \beta^2 + \frac{\omega_{f0}^2}{v^2}$$

$$\sigma_{0\to f} \approx \frac{4\pi}{3}\left(\frac{2V_0}{\hbar\omega_{f0}\beta}\right)^2 \frac{(\omega_{f0}/v\beta)^2}{[1 + (\omega_{f0}/v\beta)^2]^3}$$

Landau–Zener–Stueckleberg

(curve crossing, $\varepsilon_f + V_f = \varepsilon_0 + V_0$ at $R = R_x$)

$$P_{0\to f}(b) \approx 2\bar{P}_{0\to f}\sin^2\left[\frac{1}{\hbar}\int_0^{t_x}(\varepsilon_f - \varepsilon_0 + V_f - V_0)\, dt\right]$$

$$\bar{P}_{0\to f} = 2p_{0f}(1 - p_{0f}), \qquad p_{0f} = 1 - \exp(-\delta)$$

$$\delta = \left|\frac{2\pi}{\hbar}\Delta\varepsilon_{0f}^2 \Big/ \left(\frac{dR}{dt}\right)\frac{d}{dR}(V_f - V_0)\right|_{R=R_x}$$

$$\sigma_{0\to f} \approx \pi R_x^2 \bar{P}_{0\to f}$$

(*continues*)

TABLE III. (*Continued*)

Landau–Zener–Stueckleberg (*continued*)

Useful form: $\Delta\varepsilon_{0f} \approx V_0(R/\bar{a})\exp(-0.86R/\bar{a})$, $V_0 = (I_A I_B)^{1/2}$,

$$\bar{a} = a_0/(Z'_A + Z'_B), \qquad Z'_A \equiv \left(\frac{2a_0}{e^2} I_A\right)^{1/2}$$

Rosen–Zener (noncrossing)

$$P_{0\to f}(b) \approx \bar{P}_{0\to f} \sin^2\left[\frac{1}{\hbar}\int_{-\infty}^{\infty} \Delta\varepsilon_{0f}\, dt\right]$$

$$\bar{P}_{0\to f} = \tfrac{1}{2}\left|\frac{\int_{-\infty}^{\infty} \Delta\varepsilon_{0f}\exp(i\omega_{f0}t)\, dt}{\int_{-\infty}^{\infty} \Delta\varepsilon_{0f}\, dt}\right|^2$$

Demkov (exponential coupling, $\Delta\varepsilon_{0f} = Ae^{-R/\bar{a}}$)

$$|\Delta\varepsilon_{0f}|_{R=R_x} = \tfrac{1}{2}|\varepsilon_f - \varepsilon_0 + V_f - V_0|_{R=R_x}, \qquad \text{defines } R_x$$

$$P_{0\to f}(b) \approx \bar{P}_{0\to f} \sin^2\left[\frac{1}{\hbar}\int_0^{t_x} (\varepsilon_f - \varepsilon_0 + V_f - V_0)\, dt\right]$$

$$\bar{P}_{0\to f}(b) \approx \tfrac{1}{2}\operatorname{sech}^2\left[\frac{\pi\bar{a}}{2\hbar}(\varepsilon_f - \varepsilon_0 + V_f - V_0)/\left(\frac{dR}{dt}\right)\right]_{R=R_x}$$

$$\sigma_{0\to f} \approx \pi R_x^2 \bar{P}_{0\to f}(b)$$

Resonant charge exchange

$v \lesssim \bar{v}_e$ (Firsov)

$$P_{ct}(b) = \sin^2\left[\frac{1}{2\hbar}\int_{-\infty}^{\infty} \Delta\varepsilon(R)\, dt\right]$$

$$\sigma_{ct} \approx \tfrac{1}{2}\pi b_x^2, \quad \left[\frac{1}{2\hbar}\int_{-\infty}^{\infty} \Delta\varepsilon\, dt\right]_{b_x} \approx \pi^{-1}$$

$v \gg \bar{v}_e$ for $(H^+ + H)$

$$P_{ct} \to \frac{64\pi(b/a_0)^3}{(v/v_0)^7}\exp\left(-\frac{bv}{a_0 v_e}\right), \qquad \sigma_{ct} \propto v^{-12}$$

Langevin

$$\sigma_{0\to f} = \bar{P}_{0\to f}\pi b_0^2 \qquad [b_0 \text{ in Eq. (20)}]$$

For ion–molecule reaction:

$$b_0^2 = \frac{2}{v}\left(\frac{\alpha_B Z_A e^2}{m}\right)^{1/2}, \qquad \alpha_B = \text{polarizability}$$

Born approximation

$$\sigma_{0\to f}(\chi) = \frac{K_f}{K_0}\left[\frac{m}{2\pi\hbar^2}\int d^3R\, V_{f0}e^{i(\mathbf{K}_0 - \mathbf{K}_f)\cdot\mathbf{R}}\right]^2$$

using $V_{f0} = V_0\exp(-\beta R)$

$$\sigma_{0\to f}(\chi) = \frac{K_f}{K_0}\left[\frac{4m\beta V_0}{\hbar^2}\right]^2 \frac{1}{[\beta^2 + |\mathbf{K}_0 - \mathbf{K}_f|^2]^4}$$

$$\sigma_{0\to f} = \frac{\pi}{3K_0^2}\left[\frac{4m\beta V_0}{\hbar^2}\right]^2 \left\{\frac{1}{[\beta^2 + (K_0 - K_f)^2]^3} - \frac{1}{[\beta^2 + (K_0 - K_f)^2]^3}\right\}$$

Approximate models for the two-state impact parameter cross section in Eq. (7) can be written in the form

$$\sigma_{0\to f} \approx \bar{P}_{0\to f}\pi b_x^2 \tag{49}$$

where b_x is that impact parameter giving an onset for transitions and $\bar{P}_{0\to f}$ is an averaged transition probability. For symmetric resonant charge exchange (e.g., $H^+ + H \to H + H^+$) the probability of charge exchange is an oscillatory function at low v (Fig. 12 and Table III). The average probability of a transition (exchange) is roughly $\frac{1}{2}$ as the initial and final states are identical (i.e., $\varepsilon_0 = \varepsilon_f$). As $\Delta\varepsilon(R)$ from Eq. (38) divided by $\hbar$ is roughly the rate of electron transfer, then at large R, when the time for sharing of an electron becomes longer than the collision time, the cross section goes to zero. Firov, therefore, estimated the size of the cross section by finding the largest value of b for which the number of transfers is small,

$$\frac{1}{2\hbar}\int_{-\infty}^{\infty} \Delta\varepsilon\, dt \approx \pi^{-1} \tag{50a}$$

This is similar to the Massey–Mohr procedure used for estimating the total elastic cross section in Eq. (31). As the exchange energy at large R decreases exponentially, Eq. (50a) reduces to the well-known result

$$b_x = b_{ct} \approx \bar{a}(B - \ln v) \tag{50b}$$

where B is a very slowly varying function of v and $\bar{a}$ is the mean radius of the atomic electron cloud. Using Eq. (50b) with Eq. (49), it is seen that the charge exchange cross section increases slowly with decreasing velocity at intermediate velocities.

At very high velocities, exchange of an electron from a stationary atom to a fast ion requires a significant change in momentum. Therefore, $\bar{P}_{0\to f}$ goes to zero rapidly ($\sim v^{-12}$ for $H^+ + H$). This begins to occur for $v > \bar{v}_e$. Therefore, at high velocities the ionization cross sections dominate over the charge transfer cross sections. At very low velocities the ion and neutral can orbit due to the long-range polarization potential. Orbiting occurs at an impact parameter determined in Eq. (20), which for the polarization interaction ($n = 4$) changes as $v^{-1/2}$. As this value of b increases more rapidly with decreasing v than b_{ct} in Eq. (50b), orbiting can dominate as $v \to 0$. A schematic diagram of the net cross section over many order of magnitude of v is given in Fig. 13.

It is seen in Fig. 13 that the cross section grows even at very low velocities when $\varepsilon_f = \varepsilon_0$. On the other hand, charge exchange between nonsymmetric systems (e.g., $S^+ + O$ or $H^+ + O$) requires a small change in energy. Therefore, the cross section will exhibit a maximum as discussed above and indicated in Fig. 13. When ΔE is much greater than the state separa-

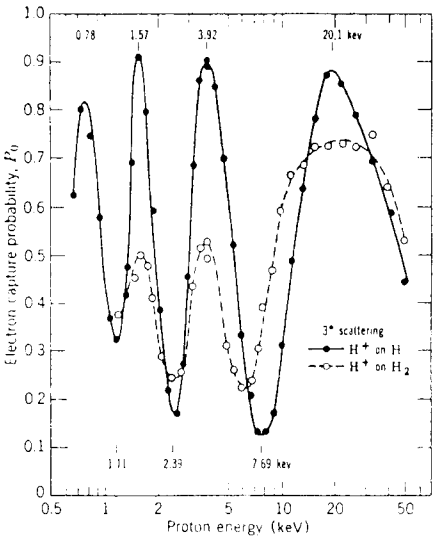

FIG. 12. Charge-exchange probability at fixed scattering angle versus incident proton energy. Peaks nearly equally spaced in v^{-1}. [From G. J. Lockwood and E. Everhart (1962). *Phys. Rev.* **125,** 567.]

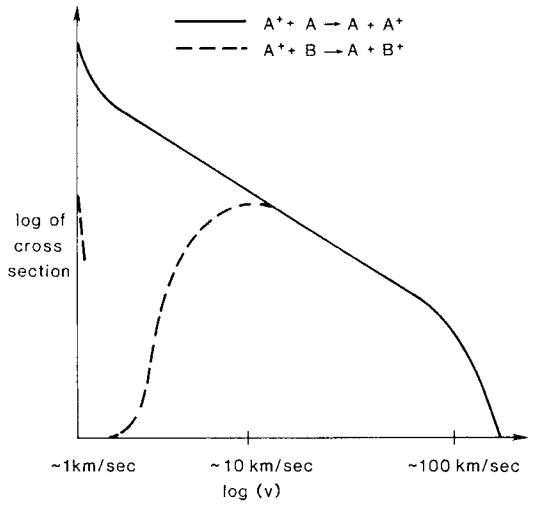

FIG. 13. Schematic diagram of the resonant and nonresonant charge exchange cross sections: decrease at very high energy due to momentum required; cross section increases with decreasing velocity at very low energies due to orbiting, for nonresonant only if exothermic.

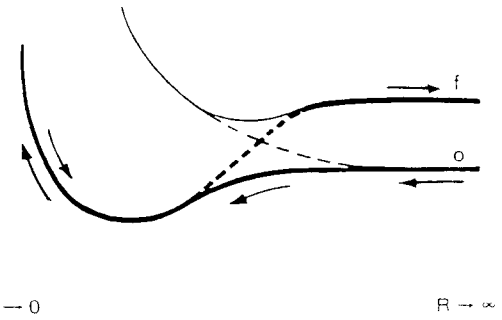

FIG. 14. Effective potentials for the two trajectories leading to a transition. Dashed lines are approximate diabatic potential curves that cross as in Fig. 8. [From R. E. Johnson (1982). "Introduction to Atomic and Molecular Collisions," p. 139. Plenum Press, New York.]

tion $|\varepsilon_f - \varepsilon_0|$, then the cross section behaves like the symmetric resonant collision [i.e., b_x given by Eq. (50) and $\bar{P}_{0\to f} \approx \frac{1}{2}$]. At velocities for which ΔE is comparable to or smaller than $|\varepsilon_f - \varepsilon_0|$, transitions generally occur in a narrow range of internuclear separations ΔR_x about a particular value R_x. In this case the transition probability is a rapidly varying function of v. Such transitions are divided into two classes, those for which a curve crossing exists (e.g., Fig. 8), and those for which the states do not cross. Therefore, knowledge of the potentials discussed earlier is required.

For the curve crossing case, b_x in Eq. (49) is set equal to the crossing point R_x. For impact parameters less than b_x, the colliding particles pass through the point R_x twice, as indicated in Fig. 14. At each passage we assign an average transition probability p_{0f} between the states. After the collision a *net* change in state will have occurred if a transition occurred on the first passage but not the second $[p_{0f}(1 - p_{0f})]$ and vice versa $[(1 - p_{0f})p_{0f}]$, yielding $\bar{P}_{0f} = 2p_{0f}(1 - p_{0f})$. Using this, Eq. (49) becomes

$$\sigma_{0f}^{LZS} \approx 2p_{0f}(1 - p_{0f})\pi R_x^2 \tag{51}$$

The fact that two different pathways lead to the same result implies inferference occurs; hence, the differential cross section is oscillatory. The Landau–Zener–Stueckleberg expression for p_{0f} is given in Table III. These expressions apply up to velocities where ΔE becomes greater than the energy splitting $|\varepsilon_f - \varepsilon_0|$, at which point the cross section behaves like the resonant case of Eq. (50). Figure 15 shows the results for three collision processes.

Demkov and Rosen and Zener have considered the case of the noncrossing interaction potentials, for example, $A^* + B \to A + B^*$. The transition region R_x is defined as that point at which the exchange interaction between the initial and final states [e.g., Eq. (38)] $\Delta\varepsilon_{0f}(R)$ is approximately equal to half the spacing between

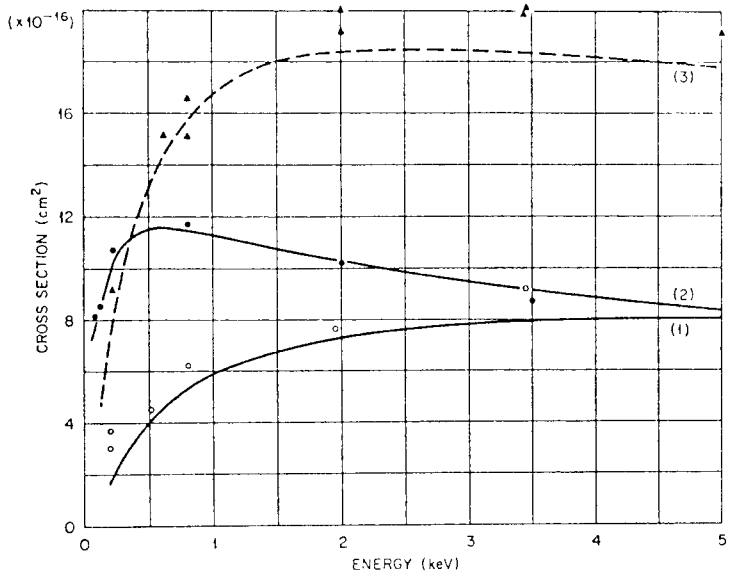

FIG. 15. Single-electron capture by doubly charged ions. Curves, LZS calculation; points are data: (1, ○) $Ar^{+2} + Ne \to Ar^{+} + Ne^{+}$; (2, ●) $N^{+2} + He \to N^{+} + He^{+}$; (3, △) $Ne^{+2} + Ne \to Ne^{+} + Ne^{+}$. [From R. A. Mapleton (1972). *Theory of Charge Exchange*, p. 212. Wiley, New York.]

states $|\varepsilon_f - \varepsilon_0 + V_f - V_0|$, where V_f and V_0 are the interaction potentials for these states [e.g., Eq. (33)]. Demkov developed a very simple and useful expression for $\bar{P}_{0\to f}$ given in Table III. The cross section so calculated would again join smoothly onto the symmetric-resonant-like result at higher velocities where the energy difference $|\varepsilon_f - \varepsilon_0|$ becomes unimportant.

At very low velocities, the cross sections for both the crossing and noncrossing cases may again increase *if the transitions are exothermic*. That is, even though the transition probability is small for any one pass through the transition region, if orbiting occurs [see Eq. (20)] then after many passes the cumulative effect can lead to a significant probability for a change in the electronic state as suggested in Fig. 13. As the collision energy is low this can only occur when internal energy is *released* due to an exothermic change in the internal state. In such a case $b_x \approx b_0$ of Eq. (20) and $\bar{P}_{0\to f}$ in Eq. (49) is equal to the statistical probability of populating any of the exothermic states.

Although we have emphasized charge-exchange collisions and, further, only collisions involving ions and atoms, these procedures apply generally to molecular collisions and to all varieties of internal change in state including molecular reactions. For example, the above discussion of orbiting applies to low-energy ion–molecule reactions yielding the often-used Langevin cross section (see Table III). In all cases, including the processes discussed here, readers are urged to refer to the specific literature for accurate measured and calculated cross sections and use the approximations here as a guide or for rough estimates when more accurate results are not available.

F. Detailed Balance

We briefly consider a property of the inelastic collision cross sections that can be quite usefully exploited in some cases. The equations of motion, both quantum-mechanical and classical, are such that

$$|f_{0\to f}(\chi)|^2 = |f_{f\to 0}(\chi)|^2$$

$$\text{or} \qquad P_{0\to f}(b) = P_{f\to 0}(b) \quad (52a)$$

This is due to the time-reversal symmetry of the collision process. Using Eq. (45b) with Eq. (52a), the differential cross sections for the forward and reverse reactions can be related. Further, integrating over angle, the integrated inelastic cross sections are related by

$$p_0^2\sigma_{0\to f}(p_0) = p_f^2\sigma_{f\to 0}(p_f) \quad (52b)$$

where p_0 and p_f are the initial and final momenta. In the semiclassical region $p_0 \approx p_f$, and therefore the forward and reverse reactions have roughly the same cross section. That is, in this region endothermic and exothermic processes behave similarly. At low velocities, near threshold for the endothermic process, the forward and reverse reactions can differ markedly as pointed out when discussing orbiting in Section VI,E. However, these processes are simply related by Eq. (52b). This relationship is a statement of the principle of detailed balance used when describing equilibrium in statistical mechanics. Based on the notions of statistical mechanics, Eq. (52b) can be extended to cases where there are a number of equivalent initial states ξ_0 and/or final states ξ_f (e.g., spin or angular momentum states),

$$p_0^2\xi_0\sigma_{0\to f}(p_0) = p_f^2\xi_f\sigma_{f\to 0}(p_f)$$

Such a relationship allows one to determine, for instance, deexcitation cross sections from data on excitation cross sections and provides a constraint when calculating cross sections by approximate methods.

G. Stopping Cross Section Summary

In the above we have considered the individual collisional processes that will determine the behavior of a fast particle penetrating a gas, liquid, or solid. The relative importance of these processes in determining the overall energy loss rate of the fast particle is illustrated in Fig. 16 for protons losing energy to H_2O. The quantity shown is the total stopping cross section $S \equiv n^{-1}(dE/dx)$ [see Eq. (11)]. First, it has been demonstrated that the molecular effects are small in the total energy loss process, so that S for H_2O is very nearly a sum of S for two H atoms and an O atom. In fact the most important difference would be that the ionization potential is lower for H_2O than for either H or O. Second, it is seen from Fig. 16 that the separate contributions, S_e and S_n, dominate the total stopping in very different velocity regions. At high velocities S_e and S_n decay as $[(\ln E_A)/E_A]$ as described above, but their magnitudes differ by the large difference in the mass of the electron versus that of the nucleus (i.e., m_e versus M_B in the denominators of the expressions for S_e and S_n; see Eq. (41b) and Table II).

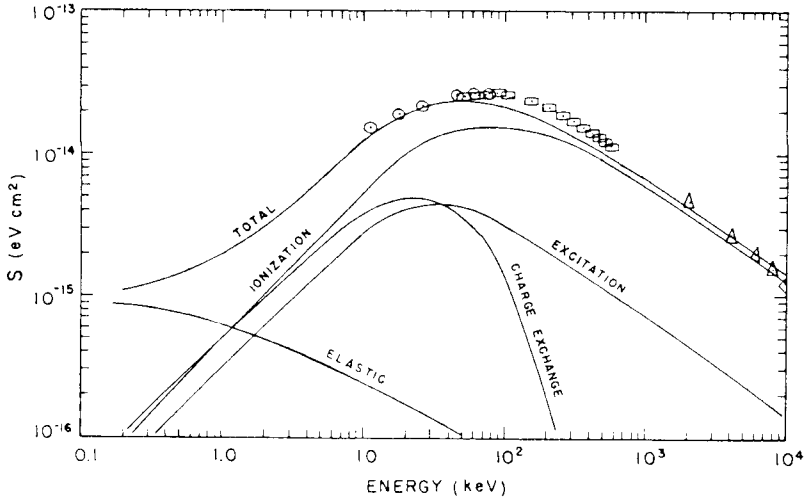

FIG. 16. Stopping cross section versus proton energy from protons incident on H_2O. Contribution from various processes (lines); experiment (points). [From J. H. Miller and A. E. S. Green (1973). *Radiat. Res.* **54,** 354.]

In the region where the electronic stopping power is large, it is seen in Fig. 16 that ionization dominates at high velocities, with a roughly 10% contribution from excitations, but charge exchange dominates at lower velocities. In this description, energy loss due to charge exchange is in fact a two-step process differing, therefore, from the other single-collision contributions shown. That is, on traversing a material, ions capture an electron, becoming neutral, and later ionize again. This process of capture and loss at low velocities can be described in the solid state as a drag force on the ion. This force comes about as the electron cloud is distorted (polarized) by the passing ion, thereby increasing the electron density in the vicinity of the ion (i.e., the covalent effect discussed earlier). The drag force produced by this distortion of the electron cloud changes roughly as $(dE/dx)_e \propto v$. Lindhard has given a very simple expression for the stopping power based on the Thomas–Fermi model of the atom that is accurate for large ions and atoms but is also reasonable for light ions and atoms for $v < \bar{v}_e$:

$$S_e \approx \xi_e 8\pi e^2 a_0 \frac{Z_A Z_B}{Z}\left(\frac{v}{v_0}\right) \qquad \xi_e \approx Z_A^{1/6}$$

In this expression v_0 is the velocity of an electron on the hydrogen atom and $Z = (Z_A^{2/3} + Z_B^{2/3})^{3/2}$.

Because the expressions given in available tables are *measurements* of S, the charge-exchange cycle is always included as the materials are macroscopically thick. This means that these tabulated values of S are *not* necessarily those of the initial charge state of the ion as it enters the solid. Because we imagine the incident ion to be in a variety of charge states during its passage through even a relatively thin material, these stopping cross sections are referred to as equilibrium-charge-state stopping cross sections. At low velocities the particle quickly becomes neutralized in the material, and at high velocities it eventually becomes fully stripped. The depth in the material at which the equilibrium charge state is achieved is related to the atomic density of the material and the average charge exchange and electron loss cross sections, all quantities we described above. This depth corresponds to hundreds of monolayers of material at high velocity and tens of monolayers at low velocities.

Transmission of ions through thin films allows us to estimate the equilibrium charge state Z_{eff}. A number of semiempirical expressions have been developed since Z_{eff} depends primarily on the ion speed. For example,

$$Z_{\text{eff}} \approx Z_A(1 + y^{-1/0.6})^{-0.6}$$
$$y \equiv 3.86\sqrt{E_A/M_A}/Z_A^{0.45}$$

with E_A in mega electron volts and M_A in atomic mass units. Such expressions for the effective charge can be used to estimate S_e by substituting Z_{eff} for Z_A in expressions for a bare incident ion, for example in Eq. (47). In fact, since I in Eq.

(47) depends primarily on the target properties, heavy ion values of S_e can be estimated from proton values of S_e by multiplying by the Z_{eff}^2 above.

BIBLIOGRAPHY

Bernstein, R. B. (1979). "Atom-Molecule Collision Theory." Plenum, New York.

Bates, D. R., and Bederson, B. (1965–1982). "Advances in Atomic and Molecular Physics," Vols. 1–18. Academic Press, New York.

Child, M. S. (1974). "Molecular Collision Theory." Academic Press, New York.

Hasted, J. B. (1972). "Physics of Atomic Collisions," 2nd ed. Am. Elsevier, New York.

Hirschfelder, J. O., Curtiss, F., and Bird, R. B. (1964). "Molecular Theory of Gases and Liquids." Wiley, New York.

Johnson, R. E. (1982). "Introduction to Atomic and Molecular Collisions." Plenum, New York.

McDowell, M. R. C., and Coleman, J. P. (1970). "Introduction to the Theory of Ion–Atom Collisions." North-Holland Publ., Amsterdam.

Massey, H. S. W. (1979). "Atomic and Molecular Collisions." Halsted Press, New York.

Massey, H. S. W., Burhop, E. H. S., and Gilbody, H. G. (1970–1974). "Electronic Ionic Impact Phenomena," 2nd ed., Vol. 1–5. Oxford Univ. Press, London and New York.

Mott, N. F., and Massey, H. S. W. (1965). "The Theory of Atomic Collisions," 3rd ed. Oxford Univ. Press, London and New York.